DOI:
10.1038/s12276-024-01195-1

Document Version
Peer reviewed version

Dysregulated CREB3 cleavage at the nuclear membrane induces karyoptosis-mediated cell death

Ga-Eun Lee[1,2], Geul Bang[3], Jiin Byun[1,2], Cheol-Jung Lee[1,4], Weidong Chen[1,2], Dohyun Jeung[1,2], Hyun-Jung An[1], Han Chang Kang[1,2], Joo Young Lee[1,2], Hye Suk Lee[1,2], Young-Soo Hong[5], Dae Joon Kim[6], Megan Keniry[7], Jin Young Kim[3], Jin-Sung Choi[1], Manolis Fanto[8], Sung-Jun Cho[9], Kwang-Dong Kim[10], and Yong-Yeon Cho[1,2]

[1]*College of Pharmacy, The Catholic University of Korea, Bucheon-si, Gyeonggi-do 14662, Republic of Korea*

[2]*BK21-4th, and RCD Control·Material Research Institute, College of Pharmacy, The Catholic University of Korea, Bucheon-si, Gyeonggi-do 14662, Republic of Korea*

[3]*Research Center for Bioconvergence Analysis, Korea Basic Science Institute, Ochang, Cheongju-si, Chungbuk 28119, Republic of Korea*

[4]*Research Center for Materials Analysis, Korea Basic Science Institute, Daejeon 34133, Republic of Korea*

[5]*Anticancer Agent Research Center, Korea Research Institute of Bioscience and Biotechnology, Cheongju-si, Chungbuk 28116, Republic of Korea*

[6]*Department of Immunology and Microbiology, School of Medicine, University of Texas Rio Grande Valley, TX 78504, USA*

[7]*Department of Biology, University of Texas Rio Grande Valley, TX 78539, USA*

[8]*Department of Basic and Clinical Neuroscience, King's College London, Maurice Wohl Clinical Neuroscience Institute, London, UK*

[9]*University of Minnesota, Department of Medicine, 420 Delaware St SE, MMC 284, Minneapolis, MN 55455, USA*

[10]*Division of Applied Life Science (BK21 four), PMBBRC, Gyeongsang National University, Jinju 52828, Korea.*

*Correspondence: Yong-Yeon Cho, Ph. D., College of Pharmacy, The Catholic University of Korea, 43,

Jibong-ro, Wonmi-gu, Bucheon-si, Gyeonggi-do 420-743, Republic of Korea. Phone: +82-2-2164-4092; Fax: +82-2-2164-4059; E-mail: yongyeon@catholic.ac.kr

Running title: CREB3-CF-induced karyoptosis

Abstract

Cancer cells often exhibit resistance to apoptotic cell death, yet they may be vulnerable to other types of cell death. Uncovering additional mechanisms governing cancer cell death is crucial for developing new therapies. Our research identifies the cyclic AMP-responsive element-binding protein 3 (CREB3) as a crucial regulator and initiator of a unique cell death mechanism known as karyoptosis. This process is marked by nuclear shrinkage, deformation, and the loss of nuclear components following nuclear membrane rupture. We found that the N-terminal domain (aa 1-230) of CREB3-full length (CREB3-FL), anchored to the nuclear inner membrane (INM), interacts with lamins and chromatin DNA. This interaction maintains a balance between the outward force exerted by tightly packed DNA and the inward constraining force, thereby preserving INM integrity. Under endoplasmic reticulum (ER) stress, aberrant cleavage of CREB3-FL at the INM leads to an abnormal accumulation of the cleaved form of CREB3 (CREB3-CF). This accumulation disrupts the attachment of CREB3-FL to the INM, resulting in a sudden rupture of the nuclear membrane and the onset of karyoptosis. Proteomic studies reveal that overexpression of CREB3-CF induces a DNA damage response akin to UVB irradiation, which is associated with cellular senescence in cancer cells. These findings demonstrate that the dysregulation of CREB3-FL cleavage is a key factor in karyoptotic cell death. Consequently, these insights offer new avenues for therapeutic strategies in cancer treatment that leverage the process of karyoptosis.

Keywords: CREB3, nuclear membrane, karyoptosis, regulated cell death, senescence

Introduction

Regulated cell death (RCD) is a form of cell death via regulatory cellular systems composed of variety of biomolecules, which is distinguishable from accidental cell death (ACD) [1-3]. Although apoptosis- and autophagy-mediated cell death are classically considered as crucial subroutines of RCD, which could induce degradation of organelles or cell death under the cellular stress and play a vital role in targeted therapy and regulation of cancer cell death [4-6], necroptosis mediated by receptor interacting serine/threonine kinase protein (RIPK) 3/MLKL is also recently classified as a regulatory cell death in cancer [7,8]. Since the incidence of malignant tumors increases greatly when excessive cell proliferation or normal cell death is inhibited, drug identification to use therapeutic agents inducing RCD is recently considered as a new foundation for cancer treatment with low toxicity [8,9]. Recent explosive expansion of RCD studies demonstrated that there are many different types of RCD with distinctive characteristics [8]. While accumulating results demonstrated that some genotoxic anticancer drugs, which generally evoke nuclear damage and DNA damage response with the loss of nuclear integrity, known effectively to induce RCD in cancer cells [6,10,11], they cannot be directly used in clinical cancer treatment because of toxic side effects in normal cells. However, the intrinsic factors and molecular mechanisms regulating nuclear integrity has not been elucidated yet.

Karyoptosis, a novel type of RCD harboring phenotypes such as nuclear shrinkage and atrophy of the cytoplasm [12], is a recently suggested terminal degradation event associated with autophagy by maladaptive, excessive excretion of nuclear components in neuronal cells [12,13]. Since apoptosis and necroptosis possess distinguishable characteristics: apoptosis - cell shrinkage, DNA fragmentation, nuclear condensation, and necroptosis - cell swelling, organelles swelling, and rupture of the plasma membrane, karyoptosis is differentiated from apoptosis and necroptosis [12,13] by forming of abnormal nuclear morphologies, including herniations, folds and crevices, fragments, and lobules [12-14]. However, intrinsic factors, extrinsic stimuli, and molecular mechanisms that trigger karyoptosis have not been identified, yet.

Cyclic AMP Response Element-Binding protein 3 (CREB3) is known as an endoplasmic reticulum (ER)/Golgi bound transcription factor [15,16]. As an activation mechanism in a canonical pathway, it is a

critical event that cleavage of the transmembrane (TM) domain of CREB3 wildtype (herein, refer to as CREB3-FL) at the Golgi complex (Gc) by S1P and S2P produces the cleaved form of CREB3 (CREB3-CF) and induces CREB3-CF nuclear accumulation [15,17]. Until now, several independent studies have focused on which CREB3 and sLZIP (herein, referred to as CREB3-dTM), an alternative splicing product of CREB3 that does not contain a transmembrane domain, involved in response to ER stress [15], Golgi stress [18], and cancer cell metastasis [19]. Moreover, abnormal nuclear morphology and nuclear membrane localization are frequently observed in ectopic expression of CREB3-FL or -CF by immunocytofluorescence (ICF) [20,21]. The roles of full-length CREB3 (CREB3-FL) and its cleaved form (CREB3-CF) in the nucleus have not been extensively studied. In this research, we present a detailed molecular and mechanistic analysis of a previously unidentified mechanism of cell death, termed karyoptosis. We found that karyoptosis is initiated through the dysregulation of the transcription factor CREB3. This dysregulation leads to the production and subsequent accumulation of CREB3-CF, which in turn increases karyoptotic cell death in cancer cells and suppresses their proliferation through cellular senescence. Furthermore, our proteomic analysis and screening of extrinsic stimuli suggest that CREB3-CF-mediated karyoptosis is driven by cell death signaling pathways. These pathways are activated by endoplasmic reticulum (ER) stress-mediated nuclear membrane and DNA damages, culminating in cell cycle arrest, cellular senescence, and eventual cell death.

Materials and Methods

Reagents

Reagents for molecular and cellular biological studies, including MG132 (cat #: C2211) and Chloroquine (CQ, cat #: S6999, Selleckchem, Houston, TX, USA), were purchased from Sigma-Aldrich (Sigma-Aldrich Korea, Gangnam, Seoul, Korea). Antibodies, including anti-Myc (cat #: sc-40), anti-cullin1 (cat #: sc-17775), anti-γH2AX (cat #: sc-517348), anti-caspase-7 (cat #: sc-81654), anti-Lamin B (cat #: sc-6216) and anti-β-actin (cat #: sc-47778), used for Western blotting, immunoprecipitation (IP), and/or immunocytofluorescence (ICF) were obtained from Santa Cruz Biotechnology (Dallas, TX, USA). Antibodies, including anti-caspase-3 (cat #: 9662S), anti-p62 (cat #: 39749), anti-PARP (cat #: 9532), anti-

RIP3 (cat #: 13526S), anti-RIP3-S227 (cat #: 93654), anti-p53 (cat #: 2527), anti-Gasdermin D (cat #: 39754), and anti-Caspase-9 (cat #: 9502) were obtained from Cell Signaling Technology (Koram Biotech Corp., Gangnam, Seoul, Korea). Anti-LC3B (cat #: NB100-2220), anti-MLKL-S358 antibodies (cat #: ab187091), and anti-Caspase-8 (cat #: NB100-56116) were obtained from Novus Biological (Minneapolis, MN, USA) and Abcam (Woburn, Cambridge, UK), respectively. Anti-CREB3 antibodies were obtained from CUSABIO (cat #: CSB-PA005948, Houston, TX, USA), FineTest (cat #: FNab01962, Wuhan, Hubei, China) or Proteintech (cat #:11275-1-AP, Rosemont, IL, USA), respectively. For pulldown antibodies, protein G Sepharose beads (cat #: 17-0618-02) were purchased from GE Healthcare (Chicago, IL, USA). Oxaliplatin (Ox, 99% pure) purchased from (MedKoo Biosciences, Morrisville, NC 27,560, USA) was directly dissolved in 10× PBS (25 μM in-stock solution). The stock solution was prepared every time before being added to the cell culture medium, and the remaining Ox stock solution was utilized within 24 h.

Cell culture

HEK293T and HeLa cells were cultured in Dulbecco's Modified Eagle's Medium (DMEM, cat #: 10-013-CV, Corning Korea, Seoul, Korea), SK-MEL-2 cells were cultured in Minimum Essential Medium supplemented with Eagle with Earle's salts & L-glutamine (MEM, cat #: 10-010-CV, Corning Korea) supplemented with 10% fetal bovine serum (FBS, cat#: 35-015-CV, Corning Korea). All cells were maintained at 37℃ in a 5% CO_2 incubator and passaged at about 90% confluency.

Expression vectors

Myc- and Flag-tag fusion proteins were constructed by basic recombinant DNA technology using pCMV-Myc from TAKARA Bio INC. (cat #: 635689, Kusatsu, Shiga, Japan) and pBICEP-CMV-2 Flag from Sigma-Aldrich (cat #: E0904, Sigma-Aldrich Korea, Gangnam, Seoul), respectively. mCherry-Lamin B (cat #:55069) and -Lamin A (cat #:55068) expression vectors were purchased from Addgene (Watertown, MA, USA). To establish stable cells expressing CREB3-CF, CREB3-dTM (also known as sLZIP), or CREB3-CF-dbZIP in SK-MEL-2, HeLa cells, and pCDH-CMV-MCS-EF1-puro viral vector were

purchased from Addgene. The expression vectors utilized in this study were confirmed by DNA sequencing before use.

Western blot and immunoprecipitation

Cell lysates (20 μg) were extracted with cell lysis buffer (cat#: TLP-121CETi, TransLab, Yuseong-gu, Deajeon, Korea), were resolved by SDS-PAGE, transferred onto PVDF membrane, and hybridized with specific antibodies as indicated. For immunoprecipitation, total lysates (150 μg) were incubated with specific antibodies (2 mg/ml) as indicated at 4℃ for 4 h or overnight. The target proteins were immunoprecipitated by adding protein G sepharose beads (GE Healthcare), incubation at 4℃ for 2 h, and centrifuging. The proteins bound in the beads were washed using washing buffer (20 mM Tris at pH 8.0, 100 mM NaCl, 1 mM EDTA, and 0.5% NP-40), boiled, and visualized by Western blotting as described above.

Ectopic expression and gene knockdown

HEK293T cells were used to produce viral particles by packaging using lentiviral or retroviral packaging systems. In brief, overexpression or knockdown viral vectors were co-transfected with packaging system vectors into HEK293T cells following guidelines provided by Addgene and cultured for 24-48 h at the 37 ℃ 5% CO_2 incubator. The medium was collected, filtered using 0.45 μm acetate syringe filters, and infected into SK-MEL-2 or HeLa cells. The infection was conducted by spreading the combined mixture containing the appropriate amount of viral particle and polybrene (final concentration of 1 μg/ml, Sigma-Aldrich) for 4-6 h and cultured overnight for stabilization of cells. The cells were then treated with puromycin (5 μg/ml) for 2-3 days, pooled, and utilized for the following experiments. The efficacy of overexpression or gene knockdown was confirmed by Western blotting.

DNA association assay

To confirm the DNA association of CREB3, we selected a RIPA buffer containing 1% Triton X-

100, 0.1% SDS, 0.5% sodium deoxycholate, 50 mM Tris-HCl pH 7.4, 150 mM NaCl, and 2 mM EDTA. Briefly, SK-MEL-2 or HeLa cells stably or transiently expressing mock, CREB3-FL, CREB3-CF, CREB3-sLZIP, were harvested, washed, and suspended in the RIPA buffer. The suspension was conducted in 15 cycles of 30-second sonication with full power/30-second resting interval to solubilize proteins including membrane integral proteins. The solubilized and chromatin-bound proteins were separated by centrifugation at 13,000 rpm for 5 minutes at 4℃ and appropriate concentration of proteins were utilized to detect chromatin-unbound and -bound CREB3 protein by western blotting.

Confocal microscopy

The cells stably or transiently expressing Myc-CREB3-CF, mutants, mCherry-EGFP-LC3B, or mCherry-Lamin A or B1 were stained with subcellular specific dyes for the Golgi complex, ER, mitochondria, and nuclei and subjected to confocal microscopy. The cells cultured in chamber slides were fixed, permeabilized using 0.5% Triton X-100/1× PBS, and blocked with 1× PBS/0.02% Tween20/1% BSA at 37℃ for 1 h. To detect the protein expression, the cells were hybridized with the anti-Myc (cat #: sc-40, Santa Cruz; cat#: 2272, Cell Signaling Technology), or γH2AX (cat #: sc-517348, Santa Cruz) overnight at 4℃ as indicated, and then hybridized with AlexaFluor-488 goat anti-mouse (cat#: A-11029, Invitrogen, Waltham, MA, USA), AlexaFluor-488 goat anti-rabbit (cat#: A-11029, Invitrogen), AlexaFluor-568 goat anti-mouse (cat#: A-11031, Invitrogen) or Alexa Fluor-647 goat anti-mouse (cat#: A-21235, Invitrogen) at RT for 1 h. The fluorescence was observed under an LSM 710 laser scanning confocal microscope (Carl Zeiss Korea Co. Ltd., Seoul, Korea), and fluorescence intensity was measured using Image J (ver. 1.53a) software (National Institutes of Health, Bethesda, MD, USA).

Transmission Electron Microscopy

Subcellular ultrastructure was observed by transmission electron microscopy. Briefly, cells were fixed in 2.5% glutaraldehyde for 2 h at 4 °C, washed with 0.1 M phosphate buffer, and fixed in 1% (wt/vol)

OsO4 in phosphate buffer. The cells were dehydrated through 50~100% ethanol for 15 min and embedded in Embed 812 Epoxy resin. After polymerization of the resin at 70°C for 48 h, serial sections were cut and mounted on formvar-coated slot grids. Sections were stained with 2% (wt/vol) uranyl acetate for 20 minutes and with lead citrate for 5 minutes. The subcellular ultrastructure of the cells was observed under a transmission electron microscope (Tecnai G2 Spirit Twin; FEI Company; Korea Basic Science Institute).

In vitro pulldown assay

His-CREB3-CF fusion proteins were partially purified by 0.5 mM IPTG induction for 4 h at 37 °C, ultrasonication lysis, and pulldown using HisPur Ni-NTA Resin (cat #: 88221, Thermo Scientific™, Waltham, MA, USA). The purified His-CREB3-CF proteins were combined with HEK293T cell lysates transiently expressed mcherry-Lamin A or -Lamin B1 and incubated overnight at 4 °C. The HisPur Ni-NTA resins were washed three times with ice-cold wash buffer (100 mM NaCl, 20 mM Tris pH 8.0, 1 mM EDTA, and 0.5% NP-40) and precipitated by centrifugation (1,000 g) at 4 °C. The precipitates were resolved by SDS-PAGE, and indicated proteins were visualized by Western blotting.

TMT 10-plex labeling and LC–MS/MS analysis

Trypsin-digested peptides were labeled using 18-plex TMT reagent according to the manufacturer's instructions (Thermo Fisher Scientific Inc., MA, USA). Peptides from the 5 different samples obtained from mock, CREB3-FL, and CREN3-CF stable cells were labeled with TMT reagents. All labeled peptides were combined and then, high pH reversed-phase liquid chromatography (RPLC) fractionation was carried out using the NexeraXR HPLC system (Shimadzu Corp., Kyoto, Japan). Briefly, the desalted peptide mixture was injected onto the Xbridge C18 column (4.6×250 mm, 5um) and fractionated using high-pH buffer A (10 mM ammonium formate in water, pH 10.0) and buffer B (10 mM ammonium formate in 90% acetonitrile, pH 10.0) into 20 fractions. All fractions were collected using an FRC-10 (Shimadzu) fraction collector. The separated peptides were collected non-contiguously, dried in a

speed vacuum, and stored at −80°C. Peptides were analyzed using an LC-MS/MS system consisting of an UltiMate 3000 RSLCnano system (Thermo Fisher Scientific) and a Orbitrap Eclipse Tribrid mass spectrometer (Thermo Fisher Scientific) equipped with a nano-electrospray source (EASY-Spray Sources, Thermo Fisher Scientific). Peptides were trapped 75 μm × 2 cm C18 precolumn (nanoViper, Acclaim PepMap100, Thermo Fisher Scientific) before being separated on an analytical C18 column (75 μm×50 cm PepMap RSLC, Thermo Fisher Scientific) at a flow rate of 250 nL/min and total run time of 95 min. Mobile phases A and B were composed of 100% water containing 0.1% formic acid and 100% acetonitrile (ACN) containing 0.1% formic acid, respectively. During the chromatographic separation, the Orbitrap mass spectrometer was operated in data-dependent mode, automatically switching between MS1 and MS2. The MS data were acquired using the following parameters: Full scan MS1 spectral (400-1600 m/z) were acquired in the Orbitrap for a maximum ion injection time of 50 ms at a resolution of 120,000 and a standard mode automatic gain control (AGC) target. MS2 spectra were acquired in the Orbitrap mass analyzer at a resolution of 30,000 with turbo-TMT setting applying high energy collision dissociation (HCD) of 36% normalized collision energy and AGC target value of 5.0×10^4 with maximum ion injection time of 54 ms. Previously fragmented ions were excluded for 20 sec. Identification and quantification of MS/MS spectra was performed using Integrated Proteomics Pipeline software with the UniProt human database (released on Apr-07-2023).

Holotomorgraphy

To measure the dynamic membrane fluctuation of karyotosis, a commercial holotomography system (HT-1X; Tomocube Inc., Daejeon, Republic of Korea) was used as previously described [22]. A diode-pumped solid-state laser (wavelength, λ=532 nm) was used as an illumination source. The beams from the laser source were split into two arms: one for the sample and the other for the reference arm. The sample beam is reflected from a digital micromirror device (DMD), and the angle of the beam impinging onto a sample is systematically controlled by projecting hologram patterns on the DMD. The diffracted beam from a sample is projected onto an image plane, where the sample beam interferes with the reference beam, and

generates hologram patterns. The phase and amplitude information were retrieved using a phase retrieval algorithm from the the multiple 2-D holograms measured at various illumination angles (N=49). Then, the 3-D RI tomogram of a cell, $n_{\text{karyotosis}}(x, y, z)$ was reconstructed using an algorithm of optical diffraction tomography. The time-lapse 2-D holograms were measured at a frame rate of 100 Hz. From the time-lapse 2-D holograms, the optical phase delay images $\Delta\phi(\text{x}, y, t)$ of a karyoptosis were measured for 256 timepoints with a frame rate of 150/s. Then, the dynamic cell height images were calculated as $\Delta h(x, y, t)=\Delta\phi(x, y, t)\cdot\lambda/(\langle n_{\text{karyotosis}}\rangle - n_{\text{m}})/2\pi$, where $\langle n_{\text{karyotosis}}\rangle$ is the mean RI of a karyoptosis, and nm is the RI of a given medium. Then, the dynamic karyoptotic cell-MFs were calculated as the root-mean-square of height difference, $\Sigma[\Delta h(x, y, t) - \langle\Delta h(x, y, t)\rangle]\ 2\ /N_{\text{frame}}$, where N_{frame} is the total number of frames. The detailed procedures can also be found elsewhere.

Statistical Information

Data are expressed as mean ± Standard Error of the Medium (SEM). GraphPad Prism 8 was used for statistical analysis. The sample sizes, reproducibility of experiments and the statistical tests used are presented in the figure legends. ZEN 3.3 on Zeiss LSM 710 confocal laser microscopy system was used for immunohistochemistry data collection and analysis. Bio-Rad ChemiDoc Touch was used for western blot data collection and analysis. BD Biosciences BD CellQuest Pro software on FACSCalibur or ModiFit LT (ver3.3) was used for Flow cytometry data collection and analysis.

Results

CREB3 is a nuclear membrane protein

Canonically, CREB3-FL is a type II membrane protein that is cleaved by S1P/S2P at the Golgi complex (Gc) [23], producing CREB3-CF [24]. Although CREB3 is known as a transcription factor belonging to bZIP superfamily [23] and regulates positively or negatively target gene expression, such as ARF4 [18,25] and PPARγ_2 [25], the effect of CREB3 in cancer cells requires further elucidation. To examine CREB3's role in cancer cell proliferation, we introduced CREB3-FL and CREB3-CF (**Supplementary Fig. 1a**) into SK-

MEL-2 melanoma cells, respectively. The surprising morphological changes (referred to here as fragility), such as nuclear DNA herniation, nuclear lobulation, and nuclear membrane ripping, were observed (**Fig. 1a**). Although CREB3-FL overexpression increased DNA herniation and led to abnormal nuclear morphology in some cells, CREB3-CF-induced fragility was not observed with to the same degree with CREB3-FL overexpression (**Fig. 1a**). In previous work, CREB3L1 (known as Oasis, a member of CREB3 subfamily), was localized to the nuclear membrane [26], CREB3-FL may have a functional role in the nuclear membrane. Western blotting using cytosolic and nuclear fractions showed that endogenous CREB3-FL and -CF were mainly detected in the nuclear fraction (**Fig. 1b**). The existence of CREB3-FL at the nuclear membrane was also confirmed by confocal microscopy using CREB3-FL and CREB3-FL-mtS1P, which is an S1P cleavage site mutant (**Fig. 1c,** and **Supplementary Fig. 1b**). Given that CREB3 interacts with DNA through its basic leucine zipper (bZIP) domain [23], it was crucial to investigate whether CREB3-FL is DNA-bound in order to ascertain if CREB3-FL is directly localized to the nuclear membrane. To investigate this, we extracted two types of proteins using RIPA buffer containing 0.1% Triton X-100, 1% SDS, and 0.5% SDOC (**Fig. 1d**). The first type includes soluble proteins, encompassing both soluble and membrane-bound proteins in the cytosol and nucleus, along with protein complexes that have weak interactions, and membrane-bound integral proteins (designated as supernatant). The second type consists of insoluble pellet proteins, which contain filamentous cytoskeletal and nuclear-skeletal proteins, as well as DNA-associated chromatin-bound proteins (designated as pellet). CREB3 proteins, including CREB3-FL, -CF, and -dTM (**Supplementary Fig. 1c)**, was mainly detected in the pellet fraction, indicating that CREB3-FL is directly localized into the nuclear membrane. This conclusion was supported by the evidence that Myc- and HA-tagged CREB3 at the N- and C-terminus, respectively, were similarly localized to the nuclear membrane (**Fig. 1e**). To determine whether the intact CREB3-FL at the nuclear membrane forms a complex with genomic DNA, we devised a scheme by CREB3-FL dissociation assay from chromatin using pellet with 1M NaCl (**Fig. 1f**). The strategy elucidated that CREB3-FL, CREB3-CF, and CREB3-FL-mtS1P were strongly bound with genomic DNA (**Fig. 1g**). Based on these results, we proposed a model in which CREB3-FL resides at the nuclear inner membrane, indicating that N-terminal 1-230 of CREB3 interacted

with nuclear DNA and the C-terminal half of CREB3-FL might localize in the intermembrane space between inner and outer nuclear membranes (**Fig. 1g**). Our data supported that CREB3-FL localized to the nuclear membrane, where it is interacted with genomic DNA via CREB3-CF.

Dysregulation of CREB3-FL cleavage ruptures the nuclear membrane

Since nuclear accumulation of CREB3-CF induced nuclear fragility (**Fig. 1a**), anchoring CREB3-FL to the nuclear membrane via TM might be vital maintaining nuclear integrity. This hypothesis was supported by the finding that CREB3-dTM showed nuclear fragility similar to CREB3-CF (**Fig 2a**). Moreover, the bZIP domain deletion of CREB3-CF (CREB3-CF-dbZIP) converted the nuclear shape from nuclear fragility to round form (**Fig. 2b**). However, CREB3-CF-dbZIP was detected in the nucleus (**Fig. 2 b** and **c**, and **Supplementary Fig. 2 a** and **b**). Taken together, these results indicated that DNA binding of CREB3-FL via the bZIP domain is indispensable for nuclear fragility. Since CREB3-CF-induced nuclear fragility also led to disperse and punctate DAPI in the cytosol (**Fig. 1a** and **2 a-c**), the nuclear integrity loss might induce DNA damage response (DDR). ICF with γH2AX antibody indicated that CREB3-CF, γH2AX, and DAPI are colocalized in microsatellites (**Fig. 2d**, *upper panels*) or cytoplasm (**Fig. 2d**, *bottom panels*), supporting this hypothesis. The robust detection of γH2AX indicated that the nuclear membrane might be ruptured or ripped. The phenomenon of the tearing-off nuclear membrane was observed by high magnification of confocal microscopy using Myc-CREB3-FL-HA overexpression (**Fig. 2e**). To compare the effectiveness of CREB3-FL and -CF on nuclear fragility, we counted nuclear fragile cells among the Myc-positive cells. The results demonstrated that CREB3-CF overexpressing cells showed the nuclear fragility in about 82% of cells, while CREB3-FL cells showed nuclear fragility in only 28% of the cells (**Fig. 2f**). The results demonstrated that DNA binding and nuclear membrane anchoring of CREB3-FL is indispensable maintaining nuclear integrity.

CREB3-CF-induced nuclear membrane ripping induces karyoptosis

CREB3-CF induced nuclear membrane ripping resulted in abnormal nuclear morphology and

DDR (**Fig. 3 a, d, e**, and **f**). As similar phenomenon is observed in progeria syndrome, a genetic disease caused by abnormal mutant Lamin polymerization [27]. CREB3-CF overexpression increased Lamin intensity (**Fig. 3a**, *left panels*) with abnormal folding and cytosolic Lamin puncta (**Fig. 3a**, *right panels*). More interestingly, when the DAPI intensity between CREB3-CF positive and negative cells was compared, CREB3-CF overexpressing cells clearly showed lower DAPI intensity compared to that of CREB3-CF negative cells (**Fig. 3a**, *graphs*). Since CREB3-FL is anchored in the nuclear membrane and the bZIP domain of CREB3-FL interacted with genomic DNA, N-terminal 1-230 of CREB3 may interact with Lamin. This hypothesis was examined by Ni-NTA pulldown assay using His-CREB3-CF and mCherry-Lamin A or B1, indicating that Lamin A and B1 interacted (**Fig. 3b**). The interaction domain of CREB3-CF was determined by IP using Myc-CREB3-CF serial deletion mutants (**Supplementary Fig. 2b**), which indicated that the bZIP domain of CREB3 interacted with Lamin B1 (**Fig. 3c**). To clarify the nuclear morphological alteration induced by CREB3-CF overexpression, we further observed the ultrastructure of subcellular organelles by TEM. SK-MEL-2 and HeLa cells stably expressing Myc-mock showed normal nuclear ultrastructure with well-dispersed chromatin, nuclear membrane, and other subcellular organelles including mitochondria (**Fig. 3d**, *top panels*). In contrast, SK-MEL-2 and HeLa cells stably expressing CREB3-CF showed a striking morphological change of the nucleus with elongation, twisted/winkled nucleus, vesicles in the nucleus, and invagination of the nuclear membrane (**Fig. 3d)**. Moreover, the nuclear membrane was deformed with a ruptured nuclear membrane by CREB3-CF overexpression in SK-MEK-2 and HeLa cells (**Fig. 3d**, *arrows in middle* and *bottom panels*). Interestingly, the invaginated vesicular areas observed in the nuclei with CREB3-CF overexpression had highly dense heterochromatin in both SK-MEL-2 and HeLa cells (**Fig. 3d**, *arrows in middle* and *bottom panels*). By holotomography using SK-MEL-2 cells transiently overexpressing mock, CREB3-FL, or CREB3-CF, we recorded live images for explosive nuclear rupture (**Fig. 3e**, and **Supplementary Live Image S3**). SK-MEL-2 cells transiently expressing CREB3-CF initially showed normal nuclear morphology (**Fig. 3e**, *frame 1*). However, the cells underwent nuclear shrinkage (**Fig. 3e**, *frame 2*), and nuclei condensed (**Fig. 3e**, *frame 3*). In frame 3, the cytoplasm was flattened and attached to the vessel surface. After this, the nucleus was explosively ruptured (**Fig. 3e**, *frame 4*). The Live

Image at the moment of the nucleus explosion clearly showed that the nuclear membrane initially formed several small nuclear membrane vesicles. An explosive wave of nuclear rupture was spread outward, likely a spray of water. The nuclear materials collapsed at the explosion sites and were engulfed by neighboring cells (**Fig. 3e**, *frame 5*). Since these cells had an explosive nuclear rupture, we referred to this type of cell death as karyoptosis.

Karyoptosis is distinguishable from apoptosis, autophagy, necroptosis, and pyroptosis

CREB3-CF expression increased γH2AX puncta in the nucleus and cytoplasm (**Fig. 2d**), indicating that karyoptosis might be associated with DDR. Unexpectedly, we found that the p53 protein level, which is canonically increased by DDR [28], was decreased by CREB3-CF expression (**Fig. 4a**). Notably, oxaliplatin, a DNA damaging anti-cancer drug, enhanced the CREB3-CF-suppressed p53 protein level (**Fig. 4b**). Simultaneously, CREB3-CF-induced γH2AX protein levels were additively increased by oxaliplatin treatment (**Fig. 4b**). The karyoptotic nucleus rupture was observed by ICF using Lamin B antibody and DAPI staining, indicating CREB3-CF induced nuclear fragility and herniation of nuclear DNA (**Fig. 4d**). These results suggested that CREB3-CF-induced DDR differs from extrinsic DDR that is induced by anti-cancer drugs, which is a hallmark of DNA damage-mediated apoptosis [29]. Based on our hypothesis, we observed that overexpressing CREB3-FL or CREB3-CF did not affect the cleavage of caspase-7, caspase-3, and Poly (ADP-ribosyl) polymerase (PARP). In contrast, treatment with etoposide did affect these factors (**Fig. 4d**), suggesting that CREB3-CF-induced karyoptosis is distinct from apoptosis. Additionally, overexpressing either CREB3-FL or CREB3-CF resulted in increased levels of p62 and cleaved LC3B-II, akin to the effects observed with chloroquine treatment, indicating that overexpression of CREB3-FL and CREB3-CF inhibits autophagy (**Fig. 4e**). This finding was further supported by ICF data showing that overexpressing CREB3-CF led to increased nuclear accumulation of LC3, a phenomenon not typically seen in canonical autophagy. Notably, CREB3-CF-induced microsatellites, which co-stained with CREB3-CF, LC3, and DAPI, were observed (**Fig. 4f**, *magnified panels*). In contrast, overexpression of CREB3-FL or CREB3-CF-dbZIP showed complete dissociation between DAPI, LC3, and CREB3 proteins

(**Fig. 4f**, *top* and *bottom panels*). These microsatellites, which formed due to CREB3-CF overexpression (Fig. 4g, ICF in left panels), were associated with an increase in extracellular vesicles (**Fig. 4g**, *TEM in right panels*), strongly suggesting a distinct mechanism from canonical autophagy in CREB3-CF-induced karyoptosis. Furthermore, overexpressing CREB3-FL or CREB3-CF did not increase the phosphorylation of RIP3 and MLKL, known biomarkers for necroptosis, in contrast to TNF-α/sMAC/zVAD (TSZ) treatment (**Fig. 4h**), indicating that CREB3-CF-induced karyoptosis is distinct from necroptosis. Additionally, overexpression of CREB3-FL or CREB3-CF did not alter Gasdermin D protein levels, unlike the LPS-treated positive control group (**Fig. 4i**), suggesting that CREB3-CF-induced nuclear rupture is distinct from pyroptosis. Collectively, these findings demonstrate that CREB3-CF-mediated karyoptosis is a distinct cellular process, differing from apoptosis, canonical autophagy, necroptosis, and pyroptosis.

ER stress triggers the cleavage of CREB3-FL and CREB3-CF production by S1P and S2P at the nuclear membrane.

Although CREB3-FL, a type II membrane protein, is primarily synthesized at the ER and processed by site-1 protease (S1P) and site-2 protease (S2P) at the Golgi complex, it appeared to be localized and cleaved at the nuclear membrane (**Fig. 1**). Therefore, identifying the external stimuli that induce CREB3-FL cleavage and CREB3-CF production is crucial. Notably, both CREB3-FL and CREB3-CF levels increased in response to UVB treatment in a dose-dependent manner (**Fig. 5a**). Additionally, ER stress-inducing vesicle trafficking inhibitors, such as brefeldin A and golgicide A, significantly enhanced CREB3-CF production, while markedly decreasing CREB3-FL levels (**Fig. 5b**). Among known ER stressors, including tunicamycin, A23187, and H_2O_2, A23187 and H_2O_2 (but not tunicamycin) elevated CREB3-CF levels (**Fig. 5c**). Intriguingly, all three stressors increased CREB3-FL protein levels (**Fig. 5c**). Direct DNA damage-inducing anticancer drugs like oxaliplatin, cisplatin, and doxorubicin did not significantly alter CREB3-FL and CREB3-CF protein levels (**Fig. 5d**), suggesting that ER stress-mediated abnormal vesicle trafficking might contribute to CREB3-FL cleavage and subsequent CREB3-CF production, leading to karyoptosis. A brefeldin A treatment/washout experiment demonstrated that increased CREB3-CF levels persisted up to 9

hours post-washout, whereas the decrease in CREB3-FL was observed at 3 hours, sustained until 9 h, and reduced at 12 h post-washout (**Fig. 5e**). This process correlated with BFA-induced ER stress and disassembly, as evidenced by reduced calregulin levels (**Fig. 5e**) and transmission electron microscopy observations (Fig. 5f). To identify potential proteases responsible for CREB3-FL cleavage into CREB3-CF, we conducted an extensive literature review and employed online prediction tools such as PeptideCutter and DNASTAR. These analyses indicated that the only potential protease sites for cleaving CREB3-FL are S1P and S2P. Notably, no specific cleavage sites typically associated with proteases like caspases, Factor Xa, Granzyme B, hydroxylamine, protein-endopeptidase, thrombin, or Tobacco etch virus protease were identified for CREB3. ICF analysis to determine the localization of overexpressed and endogenous S1P revealed that, while S1P protease was mainly detected in the cytosol, it was also present at the nucleosol and nuclear membrane (**Fig. 5g**). These findings suggested that CREB3-FL cleavage and CREB3-CF production occur at the nuclear membrane via S1P and S2P with high efficiency.

CREB3-CF-induced karyoptosis evokes DDR

Since CREB3 interacted with Lamin A and B1, CREB3 and Lamin interaction at the nuclear inner membrane might play a key role to maintain normal nuclear morphology by forming a complex with nuclear DNA and other nuclear envelope proteins [30]. Since deformation of nuclear morphology is associated with human diseases via DDR [31], nuclear integrity maintenance plays a pivotal to maintain cellular homeostasis [32]. Previous results demonstrated that UVB-induced abnormal nuclear morphology and cell death [33,34] is associated with UV-induced DNA damage [35-37] via Hutchinson-Gilford progeria syndrome (HGPS)-like abnormal nuclear shapes [38] and cellular senescence [39,40]. Since overexpression of CREB3-CF expression induced karyoptosis, which was associated with CREB3-FL anchoring and Lamin interaction at the nuclear inner membrane, proteomic study induced by CREB3-CF might identify factors and signaling cascades to induce the explosive nuclear membrane rupture. To identify the karyoptosis-involved factors and signaling cascades regulated by CREB3-CF, we designed experimental strategies to compare protein profiles using SK-MEL-2 stably expressing mock, CREB3-FL, or CREB3-CF (**Fig. 6a**). The cells were split at day four

and divided two groups. After stabilization for 24 h (Day 5), one was continuously cultured without UVB stimulation, and the other was stimulated with 10 mJ/cm^2 (**Fig. 6a**). Lysates obtained on Day 5 and at 3 h after UVB treatment were subjected to proteomic analysis. The PCA plot indicating the distribution values of changed proteins to compare the response similarity of different cells indicated that mock and CREB3-FL expressing cells were very identical (**Fig. 6b**). Moreover, when mock and CREB3-FL cells were irradiated with UVB, changed proteins of 65% in the component 1 in both cells were similarly clustered as shown in CREB3-CF (**Fig. 6b**), indicating that CREB3-CF-induced karyoptotic proteins are similarly changed as shown in that of UVB irradiation in mock or CREB3-FL cells (**Fig. 6b**). However, 13.4% of component 2 clustered proteins were differently grouped, indicating that 13.4% proteins in 64. 5% clustered 1 proteins were strongly involved in CREB3-CF-induced karyoptosis (**Fig. 6b**). Since CREB3-CF+UVB cells showed shifting to right direction from CREB3-CF cells in x-axis, the changed proteins in CREB3-CF and CREB3-CF+UVB cells may play a additive role in karyoptosis and DDR-mediated cell death (**Fig. 6b**). Volcano plot of mock or CREB3-FL cells did not show critical differences in protein profile (**Supplementary Fig. 4a**). There were only nine induced and two reduced proteins (**Supplementary Fig. 4a**). In contrast, the mock and CREB3-CF comparison showed dramatic protein profile changes. CREB3-CF increased 2,051 proteins among 4,519 counts (**Fig. 6c** and **Supplementary Table 1**). The clustering data of 2,051 proteins from CREB3-CF were distinguishable from the from mock (**Fig. 6d**). Gene ontology analysis of cluster 2 proteins that CREB3-CF increased showed that proteins involved in DNA repair and cell death were upregulated compared to mock control with significant p values (**Fig. 6e**, and **Supplementary Table 1**). The ontological classification of these proteins was categorized to six different pathways, including DDR, DDR/cell cycle checkpoint, cell death, death, programmed cell death, and cytoskeletal organization. Next, we assessed whether UVB-induced DNA damage was similar to CREB3-CF. To do this, we prepared a lysate from UVB irradiated mock cells (**Fig. 6f**). The results demonstrated that the overall pattern of increased proteins in mock+UVB cells was similar to that of CREB3-CF overexpressing cells (**Fig. 6f**). However, CREB3-CF and mock+UVB cell showed a difference in 560 proteins that were found in six gene ontology pathways, including DDR, DNA damage cell cycle checkpoint,

signal transduction in DNA damage, cell death, programmed cell death, and death (**Fig. 6 g-h**, and **Supplementary Table 2**). These indicated that CREB3-CF-initiated the karyoptosis signaling pathway shared with DDR, which was triggered by UVB, resulting in cell death.

CREB3-CF-triggered karyoptosis block cell proliferation via cellular senescence

Abnormal nuclear morphology by deformation of nuclear membrane is associated with cellular senescence as shown in HGPS [38,39]. CREB3-CF-induced karyoptosis was similarly increased the senescence associated β-gal positive cell population and β-gal intensity (**Fig. 7a**, and **Supplementary Fig. 5a**). Biochemical markers, including p21, involved in cellular senescence was dramatically increased in CREB3-CF overexpressing cancer cells (**Fig. 7b**). Notably, SK-MEL-2 cells stably expressing CREB3-CF or -dTM, but not CREB3-FL, were severely reduced cell proliferation (**Fig. 7c**, and **Supplementary Fig. 5b**). Based on the rationale that the linkage of signaling cascades between UVB-induced DDR (**Fig. 2d, 4a**, and **5**) and CREB3-CF-induced karyoptosis was suggested by the proteomic study, we further observed that UVB irradiation increased CREB3-FL and CREB3-CF (**Fig. 7d**), indicating that UVB might act as an extrinsic factor causing CREB3-CF cleavage and karyoptosis. The DDR by UVB irradiation was confirmed by increasing of γH2AX intensity and puncta (**Fig. 7e**). Notably, UVB increased DNA-bound CREB3-FL and CREB3-CF in the pellet fraction, but not in the soluble fraction (**Fig. 7f**). Surprisingly, MG132, a proteasomal degradation inhibitor, dramatically enhanced CREB3-FL and -CF protein level in both soluble and pellet fractions (**Fig. 7f**), indicating that CREB3-FL and CREB3-CF are extensively regulated by protein stability regulation with a short half-life (**Supplementary Fig. 5c**). In cell population study by cell cycle analysis, we found that low dose of UVB (5 mJ/cm^2) increased the S phase and decreased the G_1 and G_2/M phases (**Fig. 7g**). Interestingly, a dose increasing of UVB (10 mJ/cm^2) inhibited the S phase and recovered G_1 phase cells as similar to UVB non-treated group (**Fig. 7g**). At the same time, we observed that the sub-G_1 phase cells dramatically increased by 5 mJ/cm^2 UVB to 35% of the cell population (**Fig. 7g**). Unexpectedly, the sub-G1 phase cells were oppositely inhibited by 10 mJ/cm^2 UVB compared to 5 mJ/cm^2 (**Fig. 7g**) similar to a previous report [41], indicating that an unidentified cell death is existed. We assessed

cell death pathways induced by UVB using Annexin V (AV)/propidium iodide (PI) staining. We found that a low dose of UVB had reduced about 42.5% of live cell population (AV^-/PI^-). This decreasing was shared to increasing about 20% of early necrosis/necroptosis (AV^-/PI^+), about 20% of late phase cell death (also known as late apoptosis and necrosis/necroptosis, AV^+/PI^+), and about 2% of early apoptosis (AV^+/PI^-) (**Fig. 7h**), indicating that a low dose of UVB induced late phase cell death via the early necrosis/necroptosis pathway. Importantly, when UVB dose was increased to 10 mJ/cm^2, the live cell population was subsequently reduced about 23.7% (45.98% *vs.* 26.35%) and the early necrosis/necroptosis population is increased about 16% (27.59% *vs.* 43.68%, **Fig. 7f**). Moreover, since the AV^+/PI^+ population was increased just about 3% (22.56% *vs.* 25.56%), almost of SK-MEL-2 cells were floated and dead by 10 mJ/cm^2 of UVB (**Supplementary Fig. 5d**), and cell proliferation was stopped (**Fig. 7c**), we concluded that the cells arrested at the early necrosis/necroptosis phase were continuously died and discarded. Since the decreased live cell population about 62.22% by 10 mJ/cm^2 (88.51% *vs.* 26.25%) was not participated to late phase cell death (AV^+/PI^+), maximum cell death ratio for the karyoptosis via the early necrosis/necroptosis would be reached to about 43%. Importantly, confocal microscopy of SK-MEL-2 cells transiently expressing Myc-CREB3-FL-HA showed that the UVB irradiation evoked karyoptosis characteristics, including explosive nuclear membrane rupture, nuclear morphology changes, DNA herniation, and microsatellite nuclear formation correlated with the nuclear membrane rupture and the flap of the nuclear membrane in the region of herniated DNA (**Fig. 7i**). These results demonstrated that UVB is an environmental factor inducing karyoptosis. Taken together, our results demonstrated that karyoptosis directly induces cell death by explosive nucleus rupture, karyoptosis.

Discussion

Integrity regulation of the nucleus, including the assembly and disassembly of the nuclear membrane and nuclear shape maintenance, is a fundamental process to maintain life. When cells receive DNA damaging stress, including ultraviolet or ionizing radiation , DNA damage response (DDR)-inducing anti-cancer drugs, and mechanical stress that induce nuclear fragility, the cells rupture the nuclear

membrane and bulk nuclear DNA herniation, which are considered an initial process of karyoptosis that has been recently suggested as a process of regulated cell death found in the neurodegenerative disease progression [42]. Abnormal nuclear morphology, resulting from dysregulated nuclear membrane dynamics, is linked to laminopathies. These disorders are characterized by a wide array of clinically distinct phenotypes, including muscular dystrophy and progeria syndrome [43]. Additionally, these observations have important implications for cancer therapeutics. Strategies such as inducing karyoptosis and promoting cancer cell senescence could be viable approaches in cancer treatment (**Fig 7a and Supplementary Fig. 5a**). Furthermore, the regulation of metastasis by controlling membrane flexibility during cell migration, and the potential to influence cancer progression through the regulation of heterochromatin and euchromatin remodeling, thereby affecting gene expression, represent significant and relevant areas of research and therapeutic interest [43]. Although the phenotypes of karyoptosis include excessive excretion of irreplaceable nuclear components, resulting in the falling apart of the abnormal nuclear morphology, sustainable DNA damage, and atrophy of cytoplasm [12,13], the molecular initiators of karyoptosis are not clear. Our results suggest a key event at the INM that CREB3-FL may receive enzymatic cleavage at the transmembrane region, probably by the S1P/S2P intramembrane protease (**Fig. 5**). The PeptideCutter (https://web.expasy.org/peptide_cutter/) and DNASTAR analysis indicated that none of the specific cleavage sites typically associated with proteases such as caspase 1-10, Factor Xa, GranzymeB, hydroxylamine, protein-endopeptidase, thrombin, and Tobacco etch virus protease were suggested for CREB3. Based on the evidence that CREB1 was cleaved by caspase-6 and -8 [44] at the consensus amino acid sequence, ILNDLSSD, CREB3-FL cleavage was also possible by caspases. However, CREB3 lacked this consensus sequence. Interestingly, BFA, an ER stressor by inhibition of anterograde vesicle transportation from the ER to the Golgi complex, leads to increased cleavage of CREB3-FL (**Fig. 5b** and **5e**). TEM analysis clearly showed that BFA induced the ONM damage (**Fig. 5f**). Moreover, our ICF results indicated that endogenous and overexpressed S1P was observed not only cytoplasm but also nucleus, even the nuclear membrane (**Fig. 5g**). This finding suggests that when cells are stimulated with ER stress, CREB3-FL, which is located in the inner nuclear membrane, may undergo the cleavage by S1P and S2P.

Further studies to identify the extrinsic stimuli that induce CREB3-FL cleavage and CREB3-CF production demonstrated that ER stressors, such as BFA, golgicide A, calcium ionophore A23187, and UVB, induced CREB3-FL-induced CREB3-CF production. However, tunicamycin and oxaliplatin did not induce CREB3-CF production. Additionally, H_2O_2, cisplatin, doxorubicin induced weak CREB3-CF production (**Fig. 5 a-d**). This cleavage tore off tethered CREB3-FL from the nuclear membrane, resulting in the loss of equilibrated tension between the outward expansion force of packed DNA and the inward fasten force of packed DNA, triggering the explosive nuclear membrane rupture, abnormal nuclear membrane fold, and flapping nuclear membrane at a side of the nucleus. In this process, exfoliated nuclear DNA herniated to the cytoplasm will eventually trigger cell death. We defined this cell death as karyoptosis.

Our research conclusively demonstrated that two variants of CREB3, namely CREB3-dTM and CREB3-CF, which could not anchor to the inner nuclear membrane (INM), possessed the capability to induce karyoptotic nuclear fragility (**Fig. 2, 3, and 4**). These variants also impeded cell proliferation (**Fig. 7c** and **Supplementary Fig. 5b**). It is significant to note that overexpressing neither CREB3-FL nor CREB3-CF did not alter the biomarkers associated with apoptosis, autophagy, necroptosis, and pyroptosis (**Fig. 4**). Consequently, identifying biomarkers associated with CREB3-CF-induced karyoptosis is crucial for assessing the process's efficacy. In light of this, we focused on analyzing the composition of extracellular vesicles (EVs) as potential biomarkers for karyoptosis. This hypothesis was based on the observation that cytoplasmic puncta was co-stained with histone, DAPI, and CREB3 (**Fig. 2d**); LC3, DAPI, and CREB3 (**Fig. 4f**); and lamin B, DAPI, and CREB3 (**Fig. 4c**) in CREB3-CF-induced karyoptosis. Furthermore, our recent transmission electron microscopy (TEM) images reveal an increased presence of extracellular vesicles in SK-MEL-2 cells overexpressing CREB3-CF (**Fig. 4g**, *right panels*). Notably, CREB3-CF overexpression in HT-29 colon cancer cells induces the formation of budding EVs and multiple intracellular vesicles (**Fig. 4g**, *left panels*). Since the karyoptosis phenomenon induced by CREB3-CF is observable in various cell types, our findings robustly support the idea that EVs formed during karyoptosis could serve as potential biomarkers for this process. Intriguingly, a combined analysis of future additional proteomic data from extracellular vesicles and the current proteomics data (**Fig. 6**) holds great promise for identifying

biomarkers specific to karyoptosis.

Our comprehensive analysis, conducted through a population study involving nuclear fragility assessment via ICF assays, revealed that CREB3-FL and -CF exhibited karyoptosis-inducing potential of approximately 27% and 82%, respectively. This discrepancy can be attributed to two plausible explanations: (1) The process of CREB3-FL-induced nuclear fragility proceeds gradually, involving a two-step mechanism. Initially, CREB3-FL cleavage occurs, likely facilitated by S1P and S2P. Subsequently, nuclear envelope rupture occurs when a sufficient accumulation of CREB3-CF competes locally with endogenous CREB3-FL at the nuclear membrane. This cascade of events ultimately might be repaired. Therefore, small portion of cells was showed abnormal nuclear morphology (**Fig. 2f**). (2) Conversely, a substantial quantity of overexpressed CREB3-CF directly competes bulkily with endogenous CREB3-FL bound with chromatin DNA at the INM. This leads bulky dissociation of CREB3-FL from tethered nuclear membrane, resulting in the induction of bulk karyoptotic cell death (**Fig. 2f**). Since karyoptosis is evoked from the nuclear membrane integrity, which is differ from apoptosis, autophagy, necroptosis, and pyroptosis (**Fig. 4**). Since karyoptosis is suggested by the morphological characteristics, the study for the molecular biomarker identification with molecular mechanism of karyoptosis is necessary in the future.

Our previous report indicated that ultraviolet B (UVB) radiation triggers endoplasmic reticulum (ER) stress and elevates Ca^{2+} levels [45]. Additionally, certain chemotherapeutic agents, such as cisplatin and doxorubicin, along with ROS-inducing stimuli like H_2O_2, not only initiate apoptosis but also other forms of cell death, including autophagy and necroptosis [8]. Although numerous studies have linked UVB exposure to an increase in DNA damage-induced apoptosis, our findings revealed that UVB-induced cell death includes a unique form, namely karyoptosis. We utilized UVB as a karyoptosis-inducing stimulus because: (1) UVB triggers distinct cellular responses based on dosage, (2) various UVB doses can lead to carcinogenesis or increase cell death, (3) UVB induces ER stress and subsequent unfolded protein responses, and (4) UVB elevates cytosolic Ca^{2+} concentration and ROS production. Significantly, we observed that a high dose of UVB (10 mJ/cm^2) resulted in an unexpected cell population, not attributable to traditional apoptosis, constituting approximately 16-43% of cells. At the molecular level, we discovered that

maintaining a balanced tension at the nuclear inner membrane−between the expansion force of tightly packed DNA and the constraining force of the nuclear membrane−is critical for nuclear integrity. The explosive rupture of the nuclear membrane following CREB3-CF expression suggested that overexpression of CREB3-CF increases γH2AX levels, linking karyoptosis to the DNA damage response. Notably, CREB3-CF overexpression led to enhanced cellular senescence (**Fig. 7a**) and reduced foci formation (**Fig. 7c**), indicating that CREB3-CF suppresses cell proliferation. These effects were closely related to the observed increase in p21 (**Fig. 7b**) and decrease in p53 (**Fig. 4b**), suggesting that karyoptosis may utilize a p53-independent, p21-dependent signaling pathway. Further analysis of cell populations in terms of the cell cycle, sub-G_1 phase, and cell death pathways revealed that the early initiation stage of karyoptosis might share signaling pathways with other regulated cell deaths, including apoptosis, necroptosis, and autophagy. While the interactions among these regulated cell death mechanisms are not yet fully understood, UVB irradiation in CREB3-FL-overexpressing cells demonstrated sensitivity to karyoptosis (**Fig. 7i**), indicating potential manageability of this process. Thus, unraveling the molecular mechanisms of karyoptosis could offer significant potential benefits for tackling human cancer cells. Although our study currently only identified UVB and ER-stressor as extrinsic triggering stimuli, it implies that the regulatory mechanism of proteases that produce CREB3-CF through CREB3-FL cleavage could be harnessed in cancer treatment by inducing karyoptosis.

Acknowledgments

We thank Dr. Hye-Jin Kim (Tomocube Inc, Daejon, Republic of Korea) to use and technical assistant to record the Live Image of the karyoptosis using HT-X1 Holotomography. This research was supported by the Research Fund of The Catholic University of Korea (M-2023-B0002-00003); the Ministry of Science, ICT, and Future Planning (Grant No. NRF-2023R1A2C2003059; and the Alzheimer Research UK (PG2019B-008) and BBSRC International Partnership Award (1789651).

Supplementary information

The online version contains supplementary material available at http:://doi.org/XXXXXX.

Figs: Fig. S1 to S4; Tables: Tables S1 and S2; and Movies: Live Image 1 to 3

Author details

C.J.L., G.J.L., and Y.Y.C. conceived the project and Y.Y.C. supervised the project; G.E.L., H.J.A., J.I.B., W.C., and D.J. performed all the experiment except proteomics study and TET. G.B., G.E.L., C.J.L, and J.Y.K. performed the proteomic analysis; H.C.K., J.Y.L., H.S.L., and G.E.L. designed methodology and collected and reviewed the data; J.S.C., and Y.S.H. support the resource; D.J.K., M. K., M.F., S.J.C., and Y.Y.C. wrote original draft/review and editing.

Conflict of interest

The authors declare no competing interests.

References

1 Galluzzi, L. *et al.* Molecular mechanisms of cell death: recommendations of the Nomenclature Committee on Cell Death 2018. *Cell Death Differ* **25**, 486-541 (2018). https://doi.org:10.1038/s41418-017-0012-4

2 Darzynkiewicz, Z., Juan, G., Li, X., Gorczyca, W., Murakami, T. & Traganos, F. Cytometry in cell necrobiology: analysis of apoptosis and accidental cell death (necrosis). *Cytometry* **27**, 1-20 (1997).

3 Zamzami, N., Hirsch, T., Dallaporta, B., Petit, P. X. & Kroemer, G. Mitochondrial implication in accidental and programmed cell death: apoptosis and necrosis. *J Bioenerg Biomembr* **29**, 185-193 (1997). https://doi.org:10.1023/a:1022694131572

4 Fairlie, W. D., Tran, S. & Lee, E. F. Crosstalk between apoptosis and autophagy signaling pathways. *Int Rev Cell Mol Biol* **352**, 115-158 (2020). https://doi.org:10.1016/bs.ircmb.2020.01.003

5 Yang, Y. *et al.* Targeting regulated cell death with plant natural compounds for cancer therapy: A revisited review of apoptosis, autophagy-dependent cell death, and necroptosis. *Phytother Res* **37**,

1488-1525 (2023). https://doi.org:10.1002/ptr.7738

6 Chen, D. Q., Guo, Y., Li, X., Zhang, G. Q. & Li, P. Small molecules as modulators of regulated cell death against ischemia/reperfusion injury. *Med Res Rev* **42**, 2067-2101 (2022). https://doi.org:10.1002/med.21917

7 Newton, K. *et al.* Cleavage of RIPK1 by caspase-8 is crucial for limiting apoptosis and necroptosis. *Nature* **574**, 428-431 (2019). https://doi.org:10.1038/s41586-019-1548-x

8 Peng, F. *et al.* Regulated cell death (RCD) in cancer: key pathways and targeted therapies. *Signal Transduct Target Ther* **7**, 286 (2022). https://doi.org:10.1038/s41392-022-01110-y

9 Wu, J., Ye, J., Xie, Q., Liu, B. & Liu, M. Targeting Regulated Cell Death with Pharmacological Small Molecules: An Update on Autophagy-Dependent Cell Death, Ferroptosis, and Necroptosis in Cancer. *J Med Chem* **65**, 2989-3001 (2022). https://doi.org:10.1021/acs.jmedchem.1c01572

10 Woo, Y., Lee, H. J., Jung, Y. M. & Jung, Y. J. Regulated Necrotic Cell Death in Alternative Tumor Therapeutic Strategies. *Cells* **9** (2020). https://doi.org:10.3390/cells9122709

11 Qin, R. *et al.* Naturally derived indole alkaloids targeting regulated cell death (RCD) for cancer therapy: from molecular mechanisms to potential therapeutic targets. *J Hematol Oncol* **15**, 133 (2022). https://doi.org:10.1186/s13045-022-01350-z

12 Baron, O. & Fanto, M. Karyoptosis: A novel type of cell death caused by chronic autophagy inhibition. *Autophagy* **14**, 722-723 (2018). https://doi.org:10.1080/15548627.2018.1434372

13 Napoletano, F., Baron, O., Vandenabeele, P., Mollereau, B. & Fanto, M. Intersections between Regulated Cell Death and Autophagy. *Trends Cell Biol* **29**, 323-338 (2019). https://doi.org:10.1016/j.tcb.2018.12.007

14 Versaevel, M., Riaz, M., Grevesse, T. & Gabriele, S. Cell confinement: putting the squeeze on the nucleus. *Soft Matter* **9**, 6665 (2013). https://doi.org:10.1039/c3sm00147d

15 Liang, G. *et al.* Luman/CREB3 induces transcription of the endoplasmic reticulum (ER) stress response protein Herp through an ER stress response element. *Mol Cell Biol* **26**, 7999-8010 (2006). https://doi.org:10.1128/MCB.01046-06

16 Howley, B. V., Link, L. A., Grelet, S., El-Sabban, M. & Howe, P. H. A CREB3-regulated ER-Golgi trafficking signature promotes metastatic progression in breast cancer. *Oncogene* **37**, 1308-1325 (2018). https://doi.org:10.1038/s41388-017-0023-0

17 Hetz, C. & Papa, F. R. The Unfolded Protein Response and Cell Fate Control. *Mol Cell* **69**, 169-181 (2018). https://doi.org:10.1016/j.molcel.2017.06.017

18 Reiling, J. H. *et al.* A CREB3-ARF4 signalling pathway mediates the response to Golgi stress and susceptibility to pathogens. *Nat Cell Biol* **15**, 1473-1485 (2013). https://doi.org:10.1038/ncb2865

19 Kang, H., Jang, S. W. & Ko, J. Human leucine zipper protein sLZIP induces migration and invasion of cervical cancer cells via expression of matrix metalloproteinase-9. *J Biol Chem* **286**, 42072-42081 (2011). https://doi.org:10.1074/jbc.M111.272302

20 Eleveld-Trancikova, D. *et al.* DC-STAMP interacts with ER-resident transcription factor LUMAN which becomes activated during DC maturation. *Mol Immunol* **47**, 1963-1973 (2010). https://doi.org:10.1016/j.molimm.2010.04.019

21 Martyn, A. C. *et al.* Luman/CREB3 recruitment factor regulates glucocorticoid receptor activity and is essential for prolactin-mediated maternal instinct. *Mol Cell Biol* **32**, 5140-5150 (2012). https://doi.org:10.1128/MCB.01142-12

22 Sohn, M., Lee, J. E., Ahn, M., Park, Y. & Lim, S. Correlation of dynamic membrane fluctuations in red blood cells with diabetes mellitus and cardiovascular risks. *Sci Rep* **11**, 7007 (2021). https://doi.org:10.1038/s41598-021-86528-0

23 Raggo, C. *et al.* Luman, the cellular counterpart of herpes simplex virus VP16, is processed by regulated intramembrane proteolysis. *Mol Cell Biol* **22**, 5639-5649 (2002). https://doi.org:10.1128/MCB.22.16.5639-5649.2002

24 Audas, T. E., Li, Y., Liang, G. & Lu, R. A novel protein, Luman/CREB3 recruitment factor, inhibits Luman activation of the unfolded protein response. *Mol Cell Biol* **28**, 3952-3966 (2008). https://doi.org:10.1128/MCB.01439-07

25 Kim, J. & Ko, J. A novel PPARgamma2 modulator sLZIP controls the balance between

adipogenesis and osteogenesis during mesenchymal stem cell differentiation. *Cell Death Differ* **21**, 1642-1655 (2014). https://doi.org:10.1038/cdd.2014.80

26 Kamikawa, Y. *et al.* OASIS/CREB3L1 is a factor that responds to nuclear envelope stress. *Cell Death Discov* **7**, 152 (2021). https://doi.org:10.1038/s41420-021-00540-x

27 Taimen, P. *et al.* A progeria mutation reveals functions for lamin A in nuclear assembly, architecture, and chromosome organization. *Proc Natl Acad Sci U S A* **106**, 20788-20793 (2009). https://doi.org:10.1073/pnas.0911895106

28 Cho, Y. Y. *et al.* The p53 protein is a novel substrate of ribosomal S6 kinase 2 and a critical intermediary for ribosomal S6 kinase 2 and histone H3 interaction. *Cancer Res* **65**, 3596-3603 (2005). https://doi.org:10.1158/0008-5472.CAN-04-3935

29 Lu, C. *et al.* Cell apoptosis: requirement of H2AX in DNA ladder formation, but not for the activation of caspase-3. *Mol Cell* **23**, 121-132 (2006). https://doi.org:10.1016/j.molcel.2006.05.023

30 Hetzer, M. W. The nuclear envelope. *Cold Spring Harb Perspect Biol* **2**, a000539 (2010). https://doi.org:10.1101/cshperspect.a000539

31 Seelbinder, B. *et al.* Nuclear deformation guides chromatin reorganization in cardiac development and disease. *Nat Biomed Eng* **5**, 1500-1516 (2021). https://doi.org:10.1038/s41551-021-00823-9

32 Schirmer, E. C., Florens, L., Guan, T., Yates, J. R., 3rd & Gerace, L. Nuclear membrane proteins with potential disease links found by subtractive proteomics. *Science* **301**, 1380-1382 (2003). https://doi.org:10.1126/science.1088176

33 Cho, Y. Y. *et al.* RSK2 as a key regulator in human skin cancer. *Carcinogenesis* **33**, 2529-2537 (2012). https://doi.org:10.1093/carcin/bgs271

34 Wang, M. L. *et al.* Andrographolide sodium bisulfate attenuates UV-induced photo-damage by activating the keap1/Nrf2 pathway and downregulating the NF-kappaB pathway in HaCaT keratinocytes. *Int J Mol Med* **45**, 343-352 (2020). https://doi.org:10.3892/ijmm.2019.4415

35 Arul, N. & Cho, Y. Y. A Rising Cancer Prevention Target of RSK2 in Human Skin Cancer. *Front Oncol* **3**, 201 (2013). https://doi.org:10.3389/fonc.2013.00201

36 Maeda, T. *et al.* Role of p21(Waf-1) in regulating the G1 and G2/M checkpoints in ultraviolet-irradiated keratinocytes. *J Invest Dermatol* **119**, 513-521 (2002). https://doi.org:10.1046/j.1523-1747.2002.01828.x

37 Narayanan, D. L., Saladi, R. N. & Fox, J. L. Ultraviolet radiation and skin cancer. *Int J Dermatol* **49**, 978-986 (2010). https://doi.org:10.1111/j.1365-4632.2010.04474.x

38 Takeuchi, H. & Runger, T. M. Longwave UV light induces the aging-associated progerin. *J Invest Dermatol* **133**, 1857-1862 (2013). https://doi.org:10.1038/jid.2013.71

39 Wang, A. S. & Dreesen, O. Biomarkers of Cellular Senescence and Skin Aging. *Front Genet* **9**, 247 (2018). https://doi.org:10.3389/fgene.2018.00247

40 Song, J. H. *et al.* Magnolin targeting of ERK1/2 inhibits cell proliferation and colony growth by induction of cellular senescence in ovarian cancer cells. *Mol Carcinog* **58**, 88-101 (2019). https://doi.org:10.1002/mc.22909

41 Caricchio, R., McPhie, L. & Cohen, P. L. Ultraviolet B radiation-induced cell death: critical role of ultraviolet dose in inflammation and lupus autoantigen redistribution. *J Immunol* **171**, 5778-5786 (2003). https://doi.org:10.4049/jimmunol.171.11.5778

42 Rebecca Casterton, Y. H., Aitana Martinez-Cotrina, Jodi Barnard, Rhys Anderson, Sebastien Janel, Dan Solomon, Frank Lafont, Frank Hirth, Gian De Nicola, Sarah Mizielinska and Manolis Fanto. Karyoptosis mediates cell death and neurodegeneration upon proteotoxic stress. *Research Square* (2023). https://doi.org/10.21203/rs.3.rs-3287063/v1

43 Lee, G. E., Byun, J., Lee, C. J. & Cho, Y. Y. Molecular Mechanisms for the Regulation of Nuclear Membrane Integrity. *Int J Mol Sci* **24** (2023). https://doi.org:10.3390/ijms242015497

44 Francois, F., Godinho, M. J. & Grimes, M. L. CREB is cleaved by caspases during neural cell apoptosis. *FEBS Lett* **486**, 281-284 (2000). https://doi.org:10.1016/s0014-5793(00)02316-4

45 Lee, C. J., Lee, M. H., Lee, J. Y., Song, J. H., Lee, H. S. & Cho, Y. Y. RSK2-induced stress tolerance enhances cell survival signals mediated by inhibition of GSK3beta activity. *Biochem Biophys Res Commun* **440**, 112-118 (2013). https://doi.org:10.1016/j.bbrc.2013.09.042

FIGURE LEGENDS

Fig. 1 CREB3-FL is directly localized to the nuclear membrane, not canonical ER/Gc transport and S1P/S2P cleavage pathway. a Illustration showing localization CREB3-FL and -CF and nuclear morphology change. **b** Western blotting showing localization of endogenous CREB3-FL and -CF in the cytosol and nuclear fraction. **c** Illustration showing nuclear membrane localization of CREB3-FL and CREB3-FL-mtS1P. **d** *Left panels*, Diagram showing experimental strategies to obtain the extract of cytosol and nuclear fractions. *Right panels*, Western blotting showing nuclear DNA bound of CREB3-FL, -CF, and -dTM. **e** Confocal microscopy illustrating nuclear membrane localization of Myc-CREB3-FL-HA double-tagged protein. **f** Diagram showing the experimental strategy to determine the nuclear DNA binding of CREB3-FL, -CF, and -FL-mtS1P. **g** Western blotting showing nuclear DNA binding of CREB3-FL, -CF, and -FL-mtS1P by NaCl. **h** Illustration proposing localization and pose of CREB3 at the nuclear membrane.

Fig. 2 Dysregulation of CREB3-FL cleavage tears off the nuclear membrane. a Illustration showing the relationship between localization of CREB3-FL, -dTM and -CF and nuclear morphology changes. **b** ICF pictures showing the relationship between domain deletion of CREB3-CF and nuclear morphology changes. **c** ICF pictures showing the relationship between CREB3-CF serial deletion of CREB3-CF and nuclear morphology changes. **d** ICF pictures showing the effect of CREB3-FL, -CF, or -dTM on DDR, DNA herniation, and microsatellite formation. **e** Illustration showing Myc-CREB-FL-HA at the nuclear inner membrane and nuclear membrane ripping and aggregation in karyoptosis. **f** Illustration showing the frequency of nuclear abnormality by CREB3-CF expression. Error bars indicate SEM. *** $P<0.0001$ (Student *t*-test).

Fig. 3 CREB3-CF-induced nuclear membrane ripping induces karyoptosis. a Illustration showing the nuclear membrane deformation-induced nuclear DNA loss. *Left panels*, Illustration showing CREB3-CF-induced nuclear membrane deformity and loss of nuclear DNA. *Central panels*. Magnification of boxed area in left panels. *Graphs*, Comparison of DAPI intensity between CREB3-CF negative and positive cells

(n= 56-87 cells). Error bars indicate SEM. * P<0.05, ***p<0.0001 (Student *t*-test). **b** IP/Western blots indicating Lamin A and B1 interaction with CREB3-CF. c Illustration showing the interaction between bZIP domain of CREB3-CF and Lamin B1. **d** Pictures for transmission electron microscopy showing nuclear membrane abnormality in shape and integrity in mock and CREB3-CF overexpressing cells. *Arrows*, nuclear membrane deforming area with nuclear membrane invagination, and membrane integrity loss. **e** Illustration showing explosive nuclear membrane rupture in karyoptosis. Frame 1, Image showing normal nuclear morphology before karyoptosis initiation; Frame 2, Image showing initiation of karyoptosis; Frame 3, Image of karyoptosis occurring in the early stage; Frame 4, Image of the moment of karyoptotic nucleus explosion (karyoptosis); Frame 5, Image for after karyoptotic nucleus explosion. The live and time-laps video are in Supplementary Live Images, LI-S1~LI-S3.

Fig. 4 Karyoptosis is distinguishable from apoptosis, autophagy, necroptosis and pyroptosis. a Illustration showing that CREB3-CF-induced karyoptosis evokes DDR, indicating the increase of γH2AX. **b** Illustration showing that CREB3-CF-induced karyoptosis is decoupled from the p53-dependent DDR signaling pathway. **c** ICF pictures showing that un-anchoring of CREB3 at the nuclear membrane induces nuclear lobulation, invagination, and nuclear DNA herniation. **d** Western blots indicating that CREB3-CF-induced karyoptosis does not induce the cleavage of apoptosis markers. **e** Western blots indicating that CREB3-CF-induced karyoptosis inhibits autophagy. **f** ICF analysis showing that CREB3-CF overexpression increase the nuclear accumulation of LC3. **g** *ICF*, Illustration showing that CREB3-Cf increases the formation of extracellular vesicles containing CREB3-CF, lamin, and genomic DNA. *Right panels*, TEM pictures illustrating that CREB3-CF overexpression induces abnormal nuclear morphology and increases the extracellular vesicle formation. **h** Western blots showing that CREB3-CF-induced karyoptosis is differ from necroptosis. **i** Western blots showing that CREB3-CF-induced karyoptosis is distinguishable from pyroptosis.

Fig. 5. Identification of extrinsic stimuli that induce karyoptosis. a Western blot illustrating that UVB

exposure increases the endogenous protein levels of CREB3-FL and CREB3-CF. **b** Western blot analyses revealing that ER stress, induced by vesicle trafficking inhibitors like brefeldin A and golgicide A, leads to increased cleavage of CREB3-FL and subsequent production of CREB3-CF. **c** Western blot results indicating that ER stress, triggered by elevated levels of Ca^{2+} and ROS, moderately increases the protein levels of CREB3-FL and CREB3-CF, while inhibition of glycosylation does not have this effect. **d** Western blot analyses showing that direct DNA damage caused by cisplatin and doxorubicin, but not oxaliplatin, leads to a slight increase in CREB3-CF protein levels without affecting CREB3-FL protein levels. **e** Western blot analyses illustrating that the changes in protein levels of CREB3-FL and CREB3-CF over time following the washout of BFA. **f** TEM images demonstrating that BFA causes damage to the nuclear membrane. **g** ICF revealing that both overexpressed and endogenous S1P are localized not only in the cytoplasm but also at the nuclear membrane.

Fig. 6 Proteomic analysis of CREB3-CF-induced karyoptosis evokes DDR-mediated cell death. a Illustration showing sampling strategies of CREB3-CF-induced karyoptosis for proteomic analysis. Comparing strategies are analysis 1, mock and CREB3-FL; analysis 2, mock and CREB3-CF; analysis 3 CREB3-CF and mock+UVB, mock+UVB and mock, CREB3-CF and mock, and CREB3-CF/mock+UVB and mock; and analysis 4, mock+UVB and CREB3-FL+UVB. **b** Illustration showing distances of protein sets in 5 different cells in **Fig. 5a**. **c** Illustration showing hit map of CREB3-CF-induced karyoptosis by analysis 2. Red, increase; green, decrease. **d** Illustration showing protein frequency of the cluster 2 proteins in CREB3-CF-induced karyoptotic cells by analysis 2. **e** GO analysis of cluster 2 proteins of the CREB3-CF-induced karyoptotic cells by analysis 2. The detailed list is provided in Supplementary Table 1. **f** Illustration showing hit map of CREB3-CF, mock+UVB, and mock to compare CREB3-CF and mock+UVB, mock+UVB and mock, CREB3-CF and mock, and CREB3-CF/mock+UVB and mock by analysis 3. Red, increase; green, decrease. **g** Illustration showing protein frequency of the cluster 1 and 2 proteins in CREB3-CF-induced karyoptotic cells by analysis 3. **h** GO analysis of cluster 1 and 2 proteins of the CREB3-CF-induced karyoptotic cells by analysis 3. The detailed list is provided in Supplementary

Table 2.

Fig. 7 CREB3-CF-triggered karyoptosis block cell proliferation via cellular senescence. a Graphs show that cellular senescence induction by the expression of CREB3-FL or -CF. *Left*, percentage of β-gal positive cells among over 200 cells. *Right*, Fold increases of β-gal positive cells in cancer cells. The cells stained with β-gal are shown in Supplementary Fig. S5A. **b** Illustration showing that CREB3-CF induces p21 protein levels in SK-MEL-2 and HeLa cells. **c** Graphs show that expression of CREB3-CF or -dTM, but not CREB3-FL, suppresses cell proliferation in SK-MEL-2 cells. The cells stained with crystal violet are shown in Supplementary Fig. S5B. **d** Illustration showing that UVB increases CREB3-FL and -CF. **e** Illustration showing that UVB induced DDR by detection of nuclear puncta of γH2AX. **f** Illustration showing the increased nuclear DNA bound CREB3-FL and -CF by UVB irradiation. **g** Cell cycle analysis data showed that the UVB dose increasing was not matched with sub-G1 enhancement. **h** Flow cytometry data shows that early necrosis/necroptosis population is not processed to the late apoptosis/necrosis/necroptosis population. In contrast, UVB continuously decreased the live cell population in a dose-dependent manner. **i** Pictures for confocal images showing nuclear membrane ripping and rupture in CREB3-FL overexpressing cells by UVB treatment.

[Supplementary Information]

Dysregulated CREB3 cleavage at the nuclear membrane induces karyoptosis-mediated cell death

Ga-Eun Lee[1,2], Geul Bang[3], Jiin Byun[1,2], Cheol-Jung Lee[1,4], Weidong Chen[1,2], Dohyun Jeung[1,2], Hyun-Jung An[1], Han Chang Kang[1,2], Joo Young Lee[1,2], Hye Suk Lee[1,2], Young-Soo Hong[5], Dae Joon Kim[6], Megan Keniry[7], Jin Young Kim[3], Jin-Sung Choi[1], Manolis Fanto[8], Sung-Jun Cho[9], Kwang-Dong Kim[10], and Yong-Yeon Cho[1,2]

Contents:

1. Supplementary Figures: Fig. S1 to S4

Supplementary Fig. 1 Vector maps for CREB3 using Fig. 1. a Vector map for CREB3-FL and CREB3-CF for overexpression. **b** Vector map for CREB3-FL and -FL-mtS1P. **c** Vector map for CREB3-FL, -dTM and -CF.

Supplementary Fig. 2 Vector maps for Fig. 2. The vector was used in Fig. 2 a, b, c, and f. **a** Vector maps for the domain deletion mutant of CREB3-CF. **b** Vector maps for serial deletion mutants of CREB3-CF for **Fig. 2c**.

Supplementary Fig. 3 Proteomic analysis of CREB3-CF-induced karyoptosis evokes DDR-mediated cell death. a Illustration showing volcano plot of CREB3-CF-induced karyoptosis by analysis 1 illustrated in main **Fig. 6c**. Red, increase; blue, decrease. Detailed protein lists for 11 proteins are described. **b** Illustration showing volcano plot of CREB3-CF-induced karyoptosis by analysis 4 illustrated in main Fig. 6f. Red, increase; blue, decrease. Detailed protein lists for 5 proteins are described.

Supplementary Fig. 4 CREB-CF inhibits cancer cell proliferation by induction of cellular senescence. a Illustration showing that CREB3-CF expression increases cellular senescence by SA-β-gal staining in SK-MEL-2 and HeLa cells. **b** Illustration showing overexpression of CREB3-CF or -dTM suppresses cell proliferation in SK-MEL-2 cells, while cells stably expressing mock or CREB3-FL showed similar intensity of crystal violet staining. **c** Illustration showing half-life of CREB3-FL and -CF. **d** Illustration showing UVB-induced cell floating. Pictures were taken at 12 h after UVB irradiation with indicated doses.

2. Supplementary Tables: Table S1 and S2

Table S1. GOBP protein list obtained from proteomic analysis for mock and CREB3-CF (file name: Fig. 5e_proteomics-GOBP list).

Table S2. GOBP protein list obtained from proteomic analysis for CREB3-CF, mock, and mock+UVB (file name: Fig. 5h_proteomics-GOBP list).

3. Supplementary live images: Supplementary LI S1 to S3

Supplementary LI S1: Time-lapse Live Image obtained by Holotomography (HT-X1) of mock overexpression (file name: HT-X1-mock expression)

Supplementary LI S2: Time-lapse Live Image obtained by Holotomography (HT-X1) of CREB3-FL overexpression (file name: HT-X1-CREB3-FL expression)

Supplementary LI S3: Time-lapse Live Image obtained by Holotomography (HT-X1) of CREB3-CF overexpression (file name: HT-X1-CREB3-CF expression)

Fig. 1 a+b+c+d+e+f+g+h by GE Lee

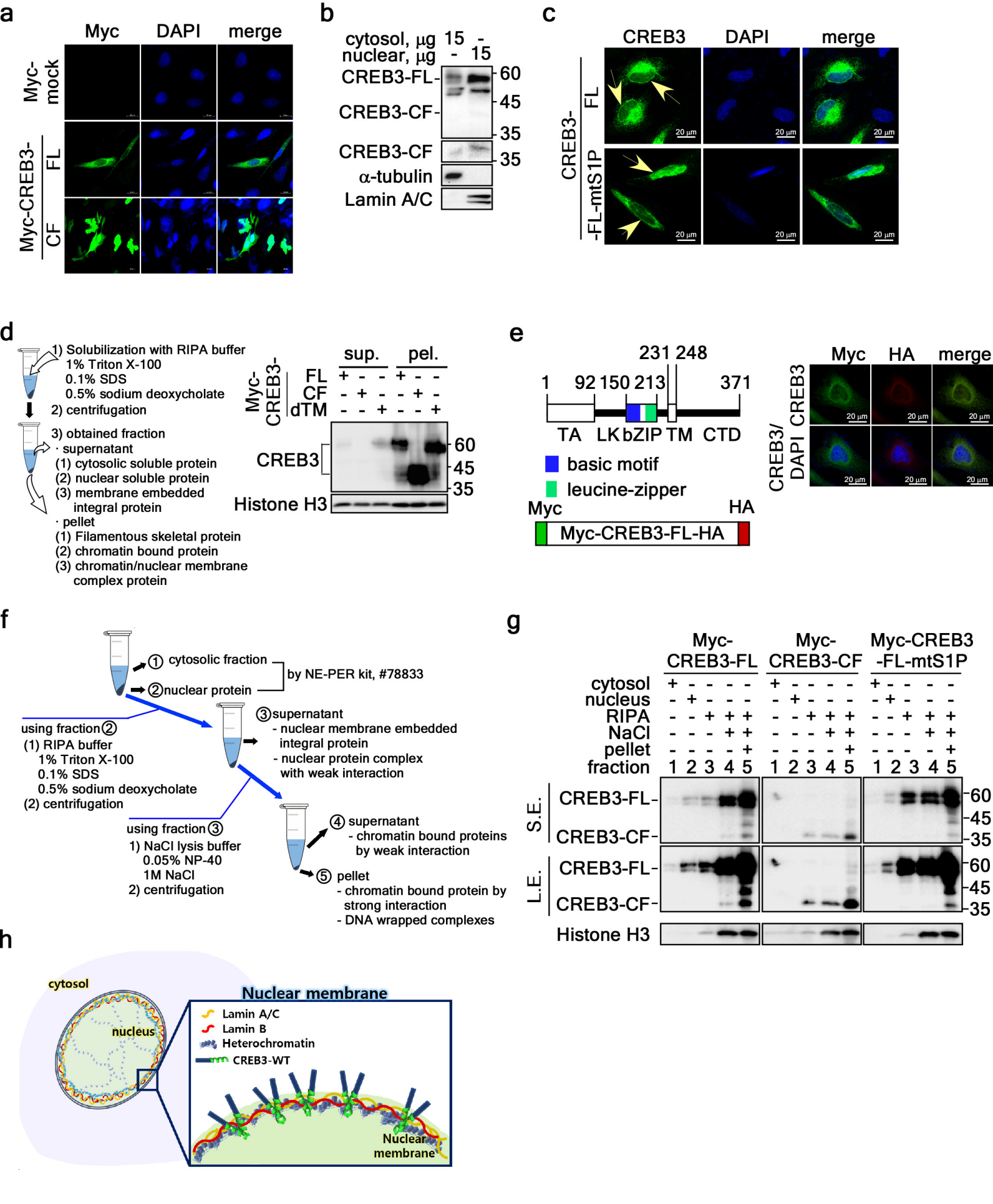

Fig. 2 a+b+c+d+e+f by GE Lee

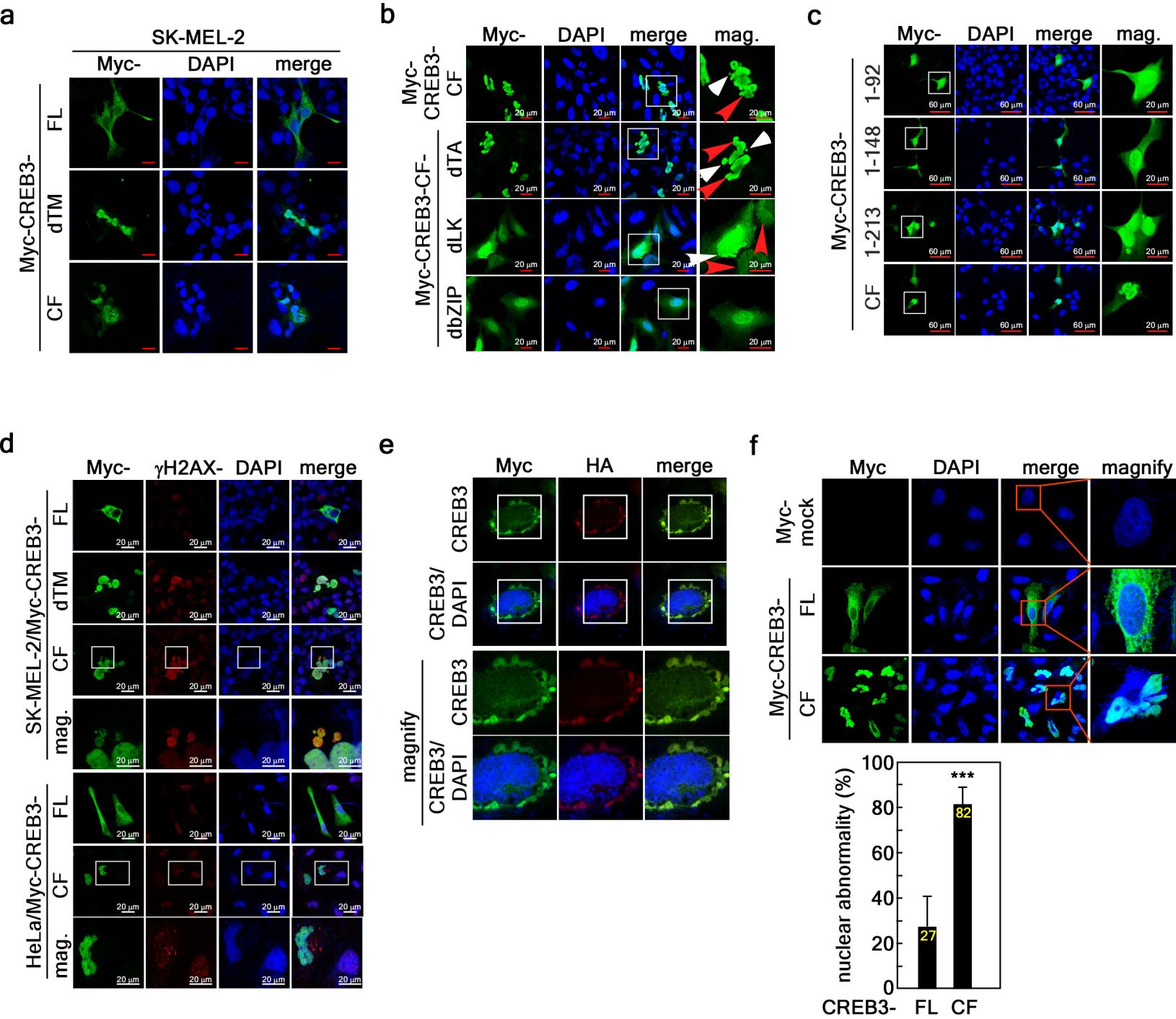

Fig. 3 a+b+c+d+e by GE Lee

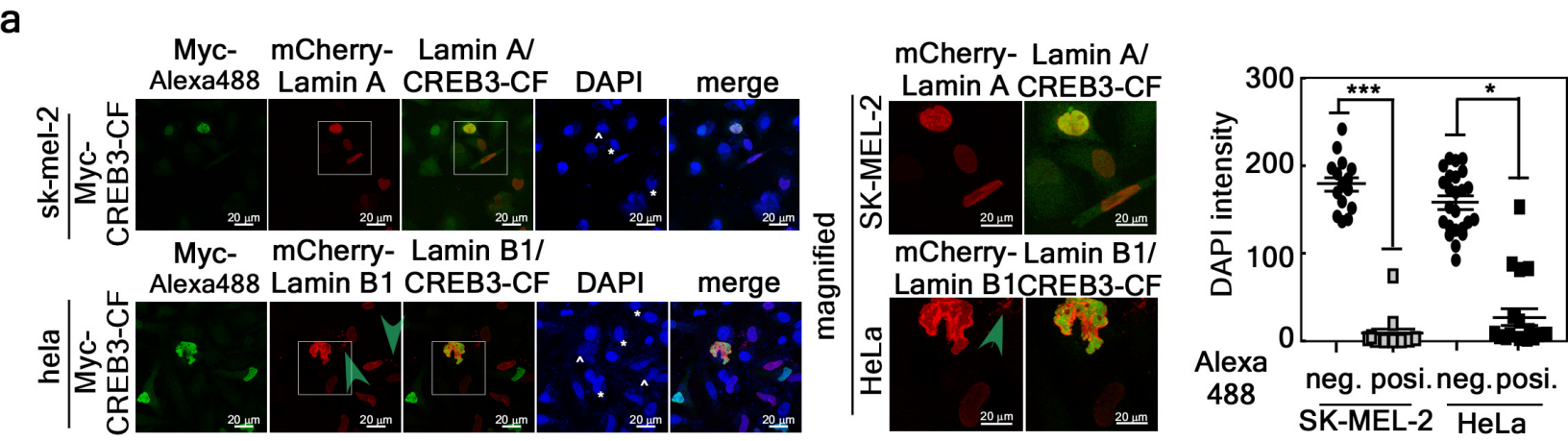

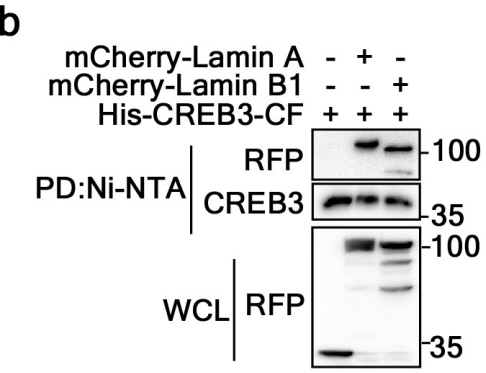

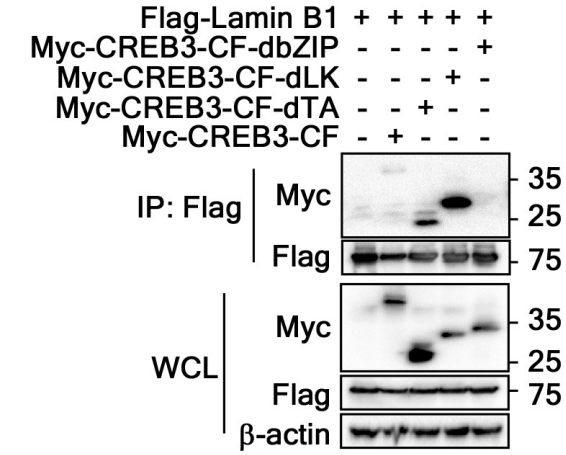

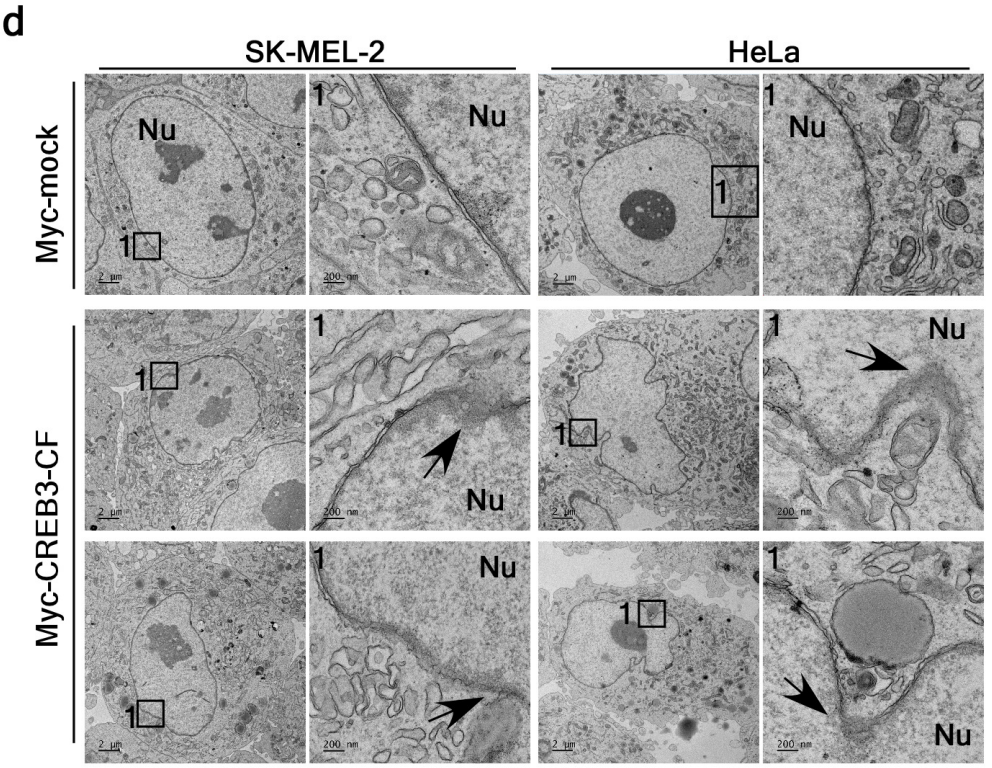

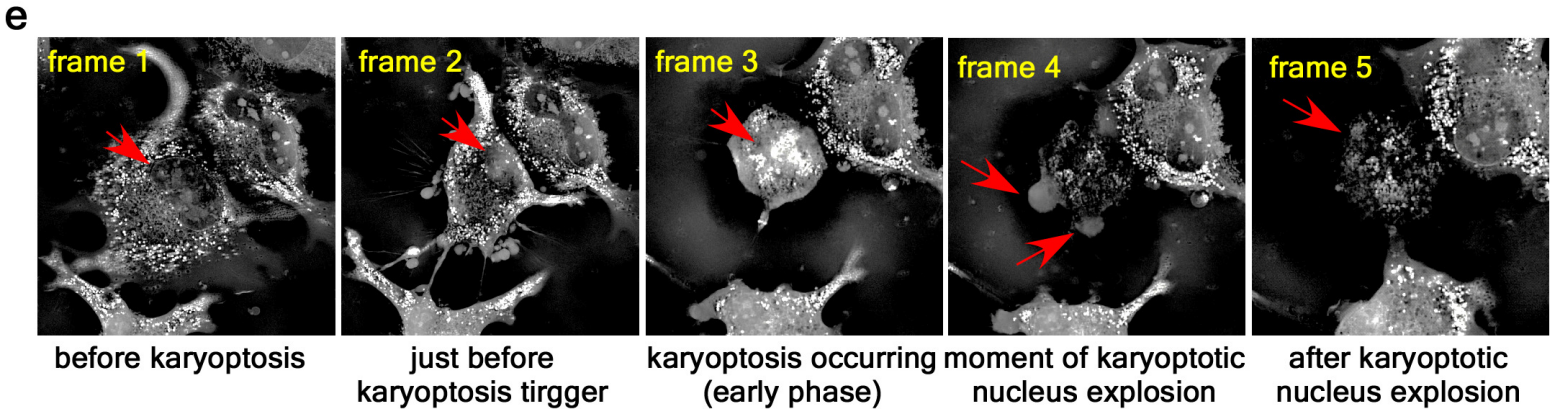

Fig. 4 a+b+c+d+e+f+g+h+i by GE Lee

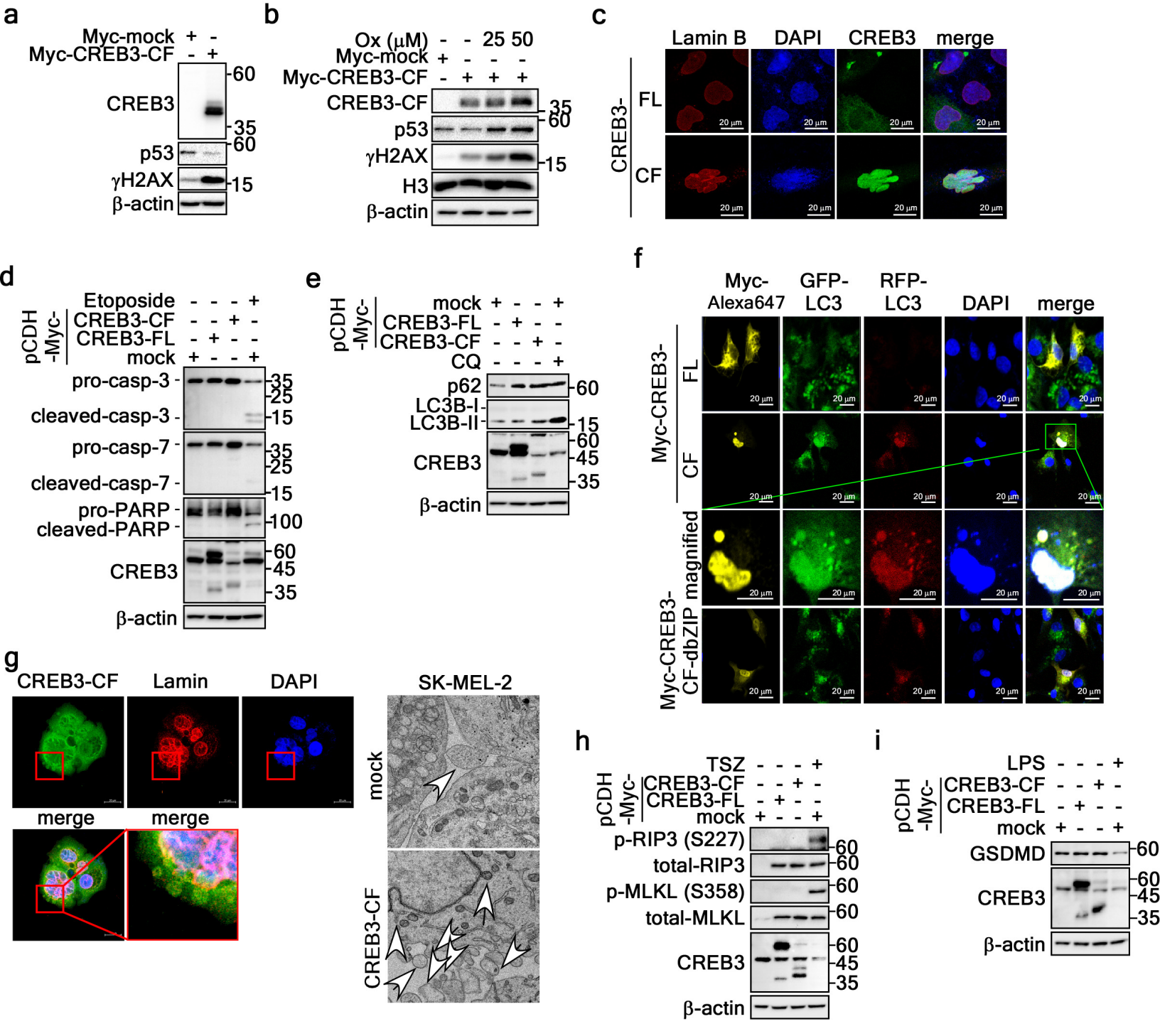

Fig. 5 a+b+c+d+e+f+g by GE Lee

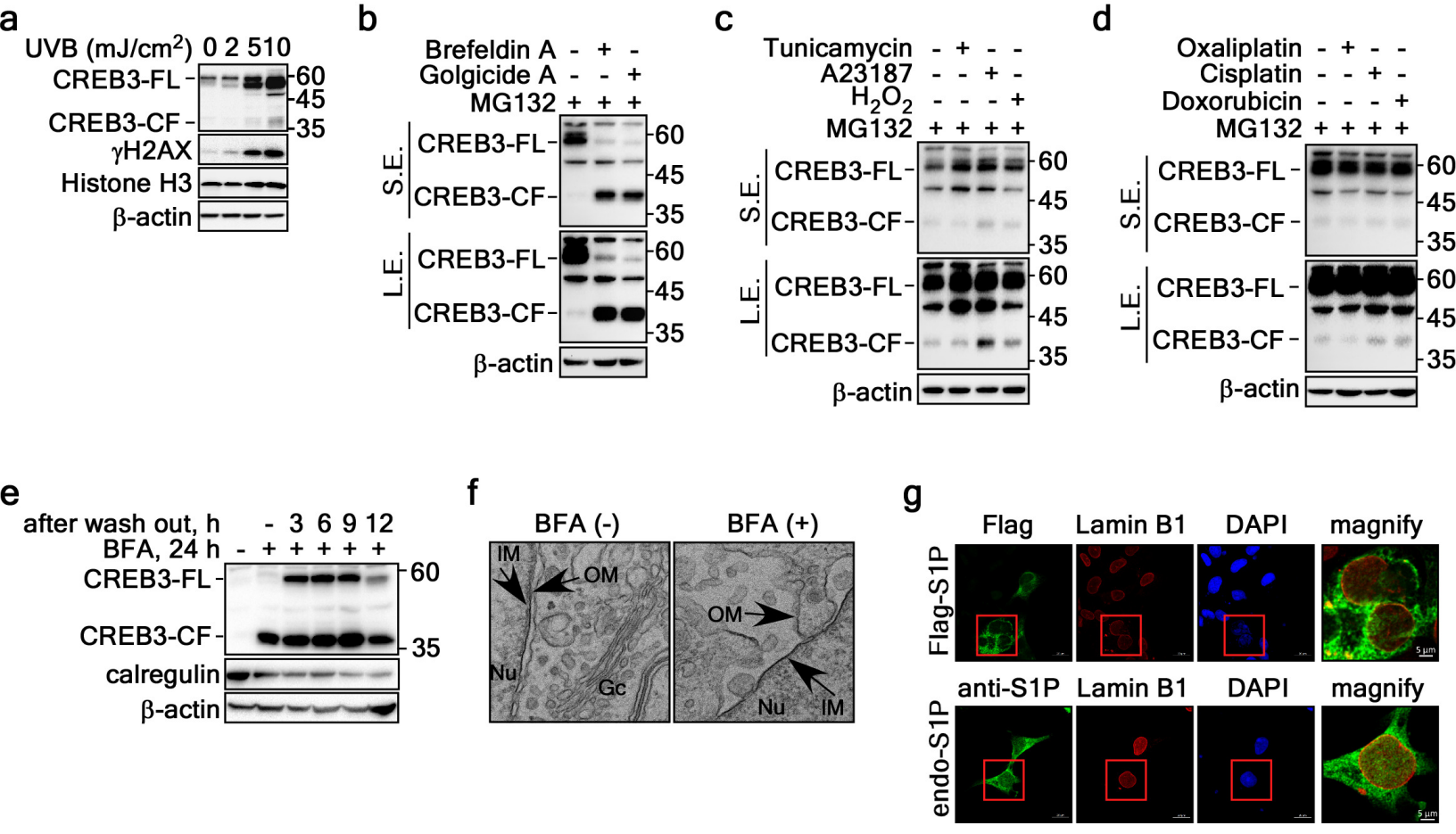

Fig. 6 a+b+c+d+e+f+g+h by GE Lee

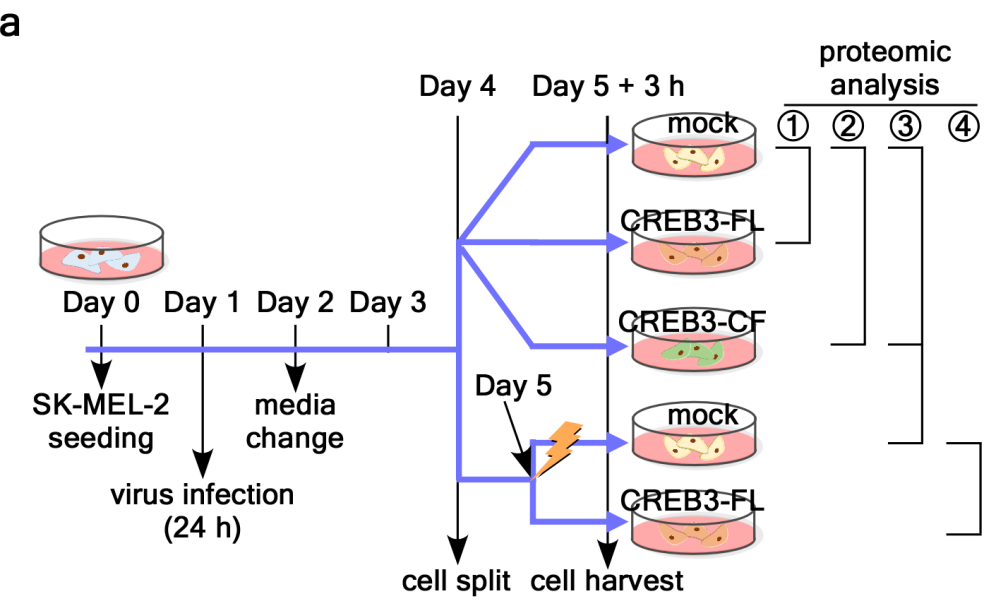

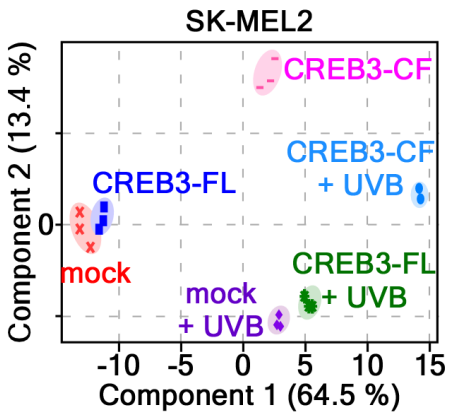

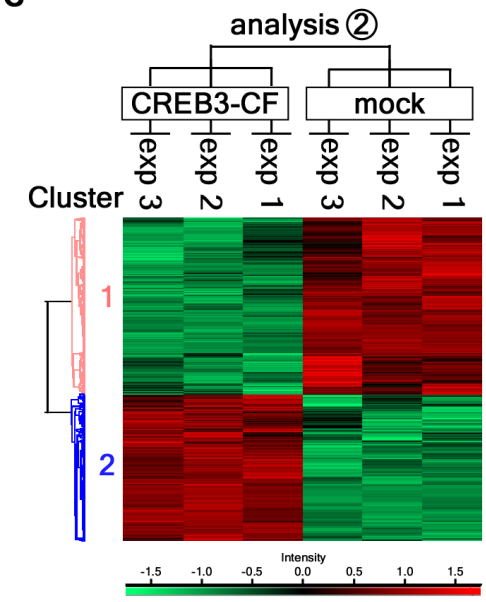

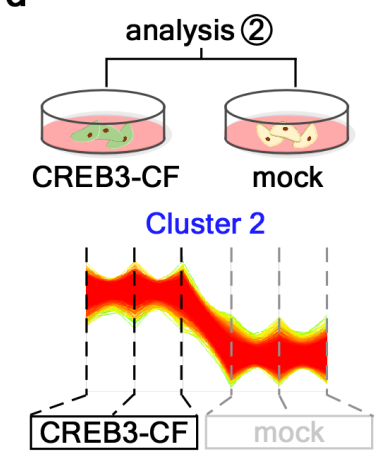

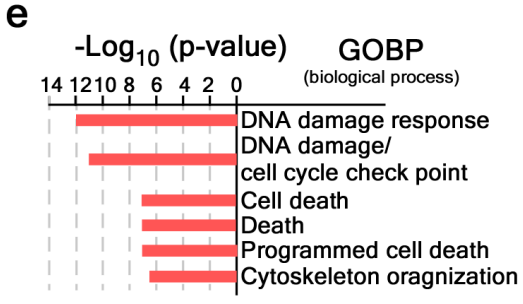

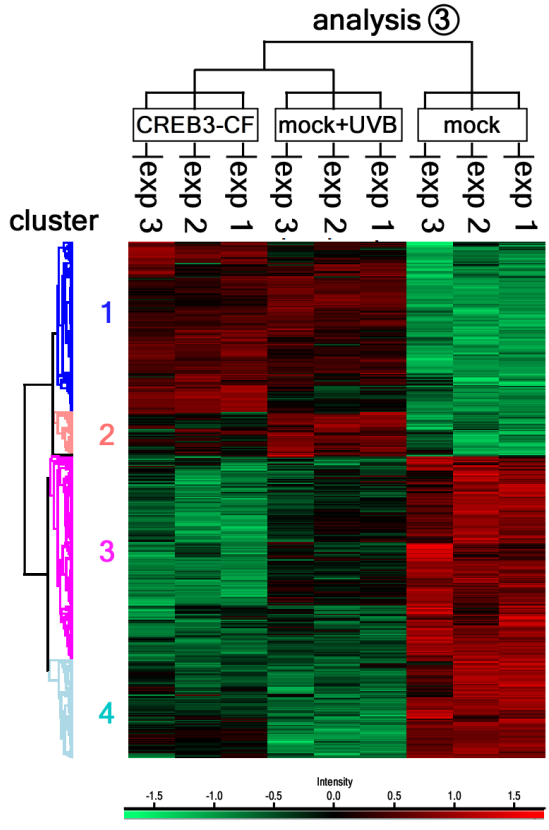

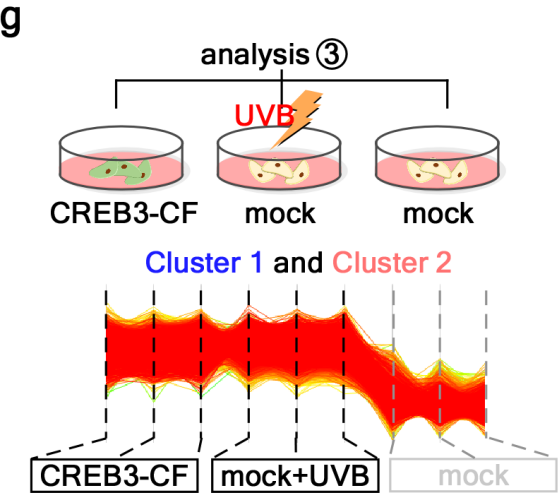

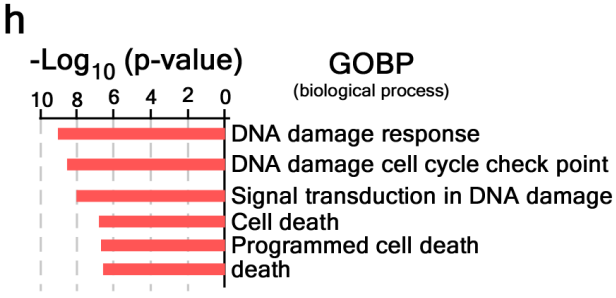

Fig. 7 a+b+c+d+e+f+g+h+i by GE Lee

a

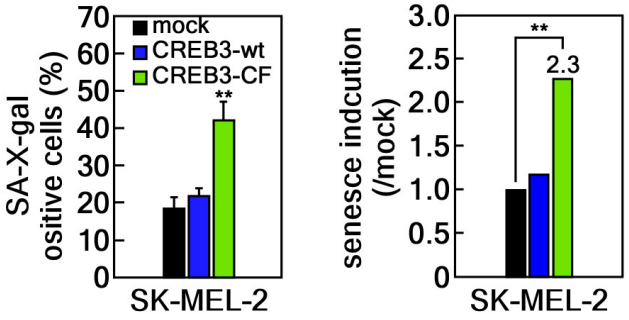

b

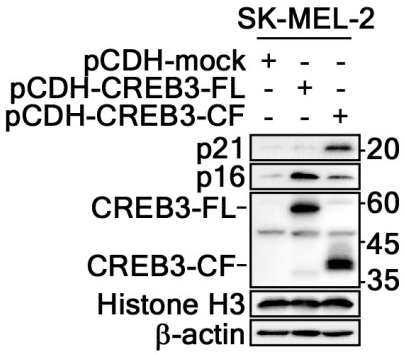

c

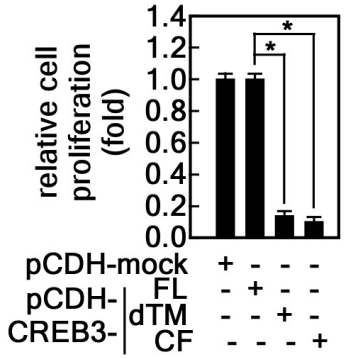

d

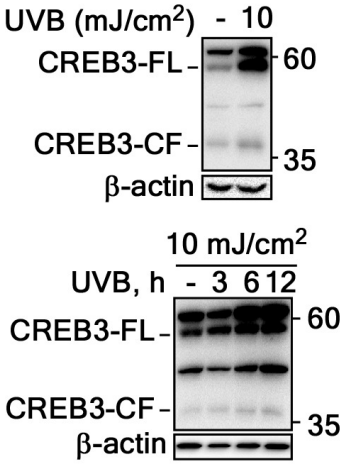

e

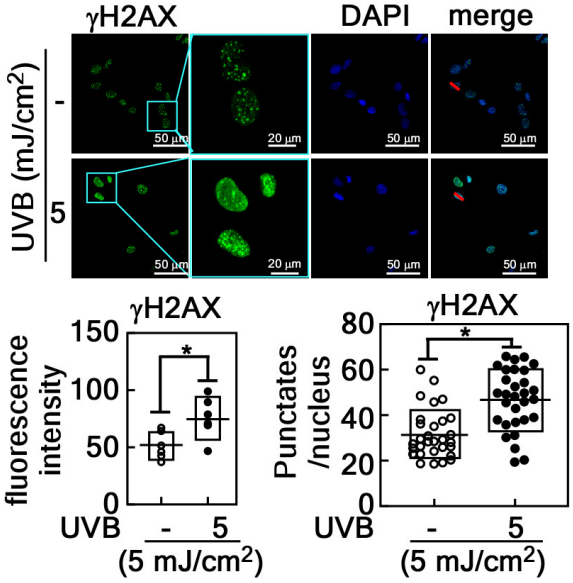

f

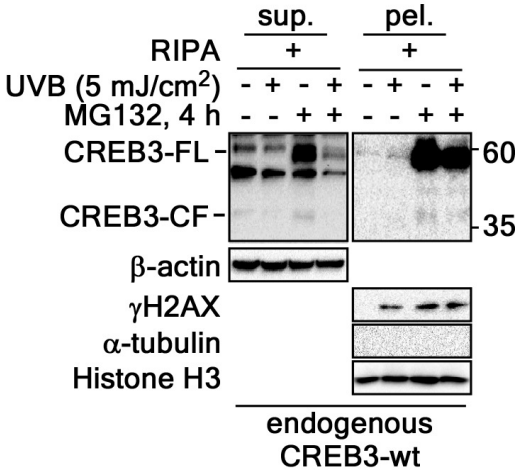

g

cell cycle phase	SK-MEL-2 UVB (mJ/cm²) (-)	5	10
sub-G1	0.0	35.0	29.6
G1	60.6	53.3	60.87
S	28.6	41.8	33.4
G2/M	10.2	4.81	5.73

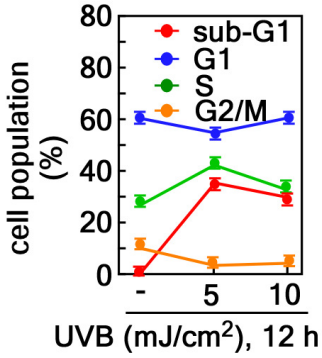

h

population catagory	SK-MEL-2 UVB (mJ/cm²) (-)	5	10
AV⁻/PI⁻	88.51	45.98	26.25
AV⁻/PI⁺	7.74	27.59	43.68
AV⁺/PI⁻	1.31	3.87	4.51
AV⁺/PI⁺	2.71	22.56	25.56

number: % of total population

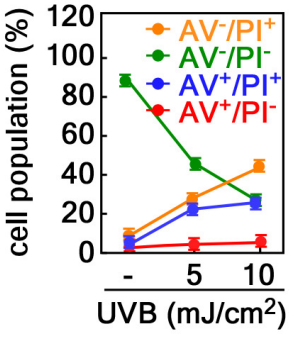

i